remote sensing

MDPI

Article

Evaluation of Sentinel-5P TROPOMI Methane Observations at Northern High Latitudes

Hannakaisa Lindqvist [1,*], Ella Kivimäki [2], Tuomas Häkkilä [2], Aki Tsuruta [3], Oliver Schneising [4], Michael Buchwitz [4], Alba Lorente [5], Mari Martinez Velarte [6], Tobias Borsdorff [6], Carlos Alberti [7], Leif Backman [3], Matthias Buschmann [4], Huilin Chen [8], Darko Dubravica [7], Frank Hase [7], Pauli Heikkinen [1], Tomi Karppinen [1], Rigel Kivi [1], Erin McGee [9], Justus Notholt [4], Kimmo Rautiainen [2], Sébastien Roche [10], William Simpson [11], Kimberly Strong [9], Qiansi Tu [12], Debra Wunch [9], Tuula Aalto [3] and Johanna Tamminen [2]

1 Space and Earth Observation Centre, Finnish Meteorological Institute, 99600 Sodankylä, Finland
2 Space and Earth Observation Centre, Finnish Meteorological Institute, 00101 Helsinki, Finland; johanna.tamminen@fmi.fi (J.T.)
3 Climate Research Programme, Finnish Meteorological Institute, 00101 Helsinki, Finland
4 Institute of Environmental Physics (IUP), University of Bremen, 28359 Bremen, Germany
5 Environmental Defense Fund, London EC3M 1DT, UK; alorente@edf.org
6 SRON Netherlands Institute for Space Research, 2333 CA Leiden, The Netherlands
7 Institute of Meteorology and Climate Research (IMK-ASF), Karlsruhe Institute of Technology, 76344 Eggenstein-Leopoldshafen, Germany
8 Joint International Research Laboratory of Atmospheric and Earth System Sciences, School of Atmospheric Sciences, Nanjing University, Nanjing 210093, China
9 Department of Physics, University of Toronto, Toronto, ON M5S 1A7, Canada
10 Environmental Defense Fund, New York, NY 10010, USA
11 Geophysical Institute and Department of Chemistry and Biochemistry, University of Alaska Fairbanks, Fairbanks, AK 99775, USA
12 School of Mechanical Engineering, Tongji University, Shanghai 200070, China
* Correspondence: hannakaisa.lindqvist@fmi.fi

Citation: Lindqvist, H.; Kivimäki, E.; Häkkilä, T.; Tsuruta, A.; Schneising, O.; Buchwitz, M.; Lorente, A.; Martinez Velarte, M.; Borsdorff, T.; Alberti, C.; et al. Evaluation of Sentinel-5P TROPOMI Methane Observations at Northern High Latitudes. *Remote Sens.* **2024**, *16*, 2979. https://doi.org/10.3390/rs16162979

Academic Editor: Carmine Serio

Received: 21 June 2024
Revised: 9 August 2024
Accepted: 11 August 2024
Published: 14 August 2024

Abstract: The Arctic and boreal regions are experiencing a rapid increase in temperature, resulting in a changing cryosphere, increasing human activity, and potentially increasing high-latitude methane emissions. Satellite observations from Sentinel-5P TROPOMI provide an unprecedented coverage of a column-averaged dry-air mole fraction of methane (XCH_4) in the Arctic, compared to previous missions or in situ measurements. The purpose of this study is to support and enhance the data used for high-latitude research through presenting a systematic evaluation of TROPOMI methane products derived from two different processing algorithms: the operational product (OPER) and the scientific product (WFMD), including the comparison of recent version changes of the products (OPER, OPER rpro, WFMD v1.2, and WFMD v1.8). One finding is that OPER rpro yields lower XCH_4 than WFMD v1.8, the difference increasing towards the highest latitudes. TROPOMI product differences were evaluated with respect to ground-based high-latitude references, including four Fourier Transform Spectrometer in the Total Carbon Column Observing Network (TCCON) and five EM27/SUN instruments in the Collaborative Carbon Column Observing Network (COCCON). The mean TROPOMI–TCCON GGG2020 daily median XCH_4 difference was site-dependent and varied for OPER rpro from −0.47 ppb to 22.4 ppb, and for WFMD v1.8 from 1.2 ppb to 19.4 ppb with standard deviations between 13.0 and 20.4 ppb and 12.5–15.0 ppb, respectively. The TROPOMI–COCCON daily median XCH_4 difference varied from −26.5 ppb to 5.6 ppb for OPER rpro, with a standard deviation of 14.0–28.7 ppb, and from −5.0 ppb to 17.2 ppb for WFMD v1.8, with a standard deviation of 11.5–13.0 ppb. Although the accuracy and precision of both TROPOMI products are, on average, good compared to the TCCON and COCCON, a persistent seasonal bias in TROPOMI XCH_4 (high values in spring; low values in autumn) is found for OPER rpro and is reflected in the higher standard deviation values. A systematic decrease of about 7 ppb was found between TCCON GGG2014 and GGG2020 product update highlighting the importance of also ensuring the reliability of ground-based retrievals. Comparisons to atmospheric profile measurements with AirCore carried out in

Sodankylä, Northern Finland, resulted in XCH_4 differences comparable to or smaller than those from ground-based remote sensing.

Keywords: methane; Arctic; boreal; TROPOMI; permafrost; TCCON; COCCON; AirCore; validation

1. Introduction

Increased greenhouse gas concentrations in the atmosphere have led to an increase of the global average temperature compared to pre-industrial times, and the change is stronger at high latitudes: the Arctic and boreal regions are warming nearly four times faster compared to the global average [1]. The changes in temperature result in a changing cryosphere [2], including contrasting regional trends of snow cover [3], degradation of permafrost [4,5], and reduced seasonal soil frost [6]. An increase in anthropogenic activity is also evident due to improved accessibility, especially for shipping [7], and expanding activity on energy production, in particular oil and natural gas extraction [8,9]. These changes may collectively result in an increase in both natural and anthropogenic high-latitude methane (CH_4) emissions that have the potential to further accelerate the ongoing changes [10,11].

Fleets of Earth-observing satellites have revolutionized the monitoring of the Arctic and boreal environments (e.g., [12,13]). For methane, passive observations in the thermal infrared spectral range have been carried out by multiple missions (e.g., AIRS, IASI, and TES). While these missions are particularly relevant for high-latitude observations because the retrievals do not require solar radiation, to infer information about the emissions near the surface demands a sensitivity of the instrument to the boundary layer of the atmosphere that is not achievable using thermal infrared wavelengths. Global observations of atmospheric methane in the near-infrared wavelengths started in 2002 with SCIAMACHY onboard ENVISAT [14]. In 2009, JAXA's Greenhouse Gases Observing Satellite (GOSAT; [15]) became the first satellite dedicated to atmospheric greenhouse gas observations. GOSAT observations have enabled an improved understanding of methane emissions and their trends globally (e.g., [16,17]) and have contributed to the quantification of emissions, specifically over high latitudes [18]. The observational high-latitude coverage of satellites has most recently been augmented by the launch of the Dutch Tropospheric Monitoring Instrument (TROPOMI; [19]) onboard the European Space Agency's Sentinel 5 Precursor satellite in November, 2017. A wide swath and a medium-resolution pixel size have enabled the use of these observations for data-driven emission estimations (e.g., [20–22]), even at higher latitudes [23].

Despite the major increase in the quantity and coverage of methane observations in the Arctic, high latitudes have not been a focus in retrieval algorithm development that has rightfully aimed for a globally optimal accuracy and precision of the retrieval products. High latitudes impose a number of challenges for passive observations of near-infrared radiation and the retrieval of a column-averaged dry-air mole fraction of methane (XCH_4) at these wavelengths. The most significant challenge is the seasonal lack of solar radiation, the solar elevation varying from large solar zenith angles (SZAs) to polar night conditions north of the Arctic circle (about 66°34′N). Large SZAs lead to an increase in atmospheric scattering and, thus, complicate the estimation of the path length of radiation in the atmosphere. Another challenge is posed by snow-covered surfaces. While snow is highly reflective in the UV-VIS wavelengths, its reflectance decreases significantly in the near-infrared wavelengths due to the absorption by ice crystals (e.g., [24,25]). This means that, over snow-covered surfaces, the reflected radiances measured by the satellite instruments are already low due to large SZAs and are further reduced by the absorption of the surface, lowering the signal-to-noise ratio and complicating the retrievals of XCH_4. The third challenge specific to high-latitude observations of methane is the polar stratospheric vortex, which is a re-occurring meteorological phenomenon in the stratosphere. In winter, the polar

vortex develops above the North Pole, and creates a stable system of little air exchange with the surrounding atmosphere. The air masses that descend within the polar vortex are depleted in methane, due to the oxidation of methane over time since the air entered the stratosphere. The descent of air affects the atmospheric profile of methane, and can thus impact retrievals through their a priori profiles that may deviate from the true profile shape [26–28]. An important opening to high-latitude-specific retrieval improvements was presented recently by Hachmeister et al. [29], who updated the digital elevation model (DEM) used in the TROPOMI retrievals of column-XCH_4, resulting in improved data over the high latitudes, especially over regions with steep altitude changes, such as Greenland.

Satellite observations of methane provide a valuable resource for monitoring and understanding the ongoing changes in the Arctic-boreal region but information on the reliability of the retrieval products specifically at high latitudes is necessary. In this paper, a systematic evaluation of TROPOMI XCH_4 products is performed. The products are derived from two different Level 2 processing algorithms: the operational product (OPER; [30–33]) and the scientific product (WFMD; [34,35]), including the evaluation of recent version changes of each product (OPER, OPER rpro, WFMD v1.2, and WFMD v1.8). The purpose of the paper is to benchmark the existing products and evaluate the information they provide for high-latitude emission-related studies, as well as quantify their differences. Using ground-based reference measurements, an evaluation of the product accuracy and precision is made. The present study is structured as follows. The satellite data as well as the ground-based validation data are described in Section 2. The methods used in the analysis are presented in Section 3. Results are presented and discussed in Section 4, and conclusions are drawn in Section 5.

2. Data Description

2.1. TROPOMI XCH_4 OPER and OPER Rpro Products

The TROPOMI operational XCH_4 retrieval product is produced by the SRON Netherlands Institute for Space Research. The product provides methane column concentrations retrieved from TROPOMI radiance measurements using the RemoTeC algorithm. The retrieval algorithm RemoTeC has been extensively used to retrieve XCO_2 and XCH_4 columns from, e.g., OCO-2 and GOSAT measurements [36,37], and is also the operational algorithm for the Sentinel-5 mission. The RemoTeC algorithm deploys a full-physics forward simulation to simulate spectral measurements of the instrument for different atmospheric conditions, accounting for scattering of aerosols. It is based on a Tikhonov profile retrieval scheme in combination with an iterative optimization that adjusts the model parameters until the best fit between the model and the measured data is achieved [38,39]. The TROPOMI operational XCH_4 product uses CH_4 and CO a priori vertical profiles from the global chemical transport model TM5 [40]. The output of the inversion is a vertical profile, which is then integrated along the vertical direction to provide the total vertical column.

Methane retrievals are only performed for cloud-free ground pixels that fulfill certain criteria in terms of viewing geometry or surface roughness. To identify cloud-free scenes, the algorithm uses the re-gridded Visible Infrared Imaging Radiometer Suite (VIIRS) cloud mask from the Suomi-NPP satellite, flying in a constellation 3.5 min ahead of the Sentinel-5 Precursor. The detailed filtering criteria of the pre-filter along with other details of the algorithm are given in the Algorithm Theoretical Baseline Document for Sentinel-5 Precursor methane retrieval [41] document.

The operational TROPOMI XCH_4 retrieval product [30] consists of versions v01.02.02–v01.04.00 (1 January 2018–3 July 2021) and v02.02.00–v02.03.01 (6 July 2021–31 December 2021), and is, in this paper, referred to as OPER. A reprocessing of the full data record was carried out in 2023 following changes introduced by Lorente et al. [31], including, for example, a second-order polynomial update for an improved representation of the surface reflectance's spectral dependence [42]. This reprocessed operational product consists of version 02.04.00, and is, in this paper, referred to as OPER rpro.

For the correct usage of the OPER and OPER rpro data products, the recommendation to use TROPOMI XCH_4 bias-corrected data associated with a quality assurance value qa_value > 0.5 is followed. The qa_value is included as part of the XCH_4 data product and provides information about the data quality and reliability of the retrieval. It ranges from 0 to 1, for non-convergent or pre-filtered pixels to convergent or clear-sky pixels, respectively.

2.2. TROPOMI XCH_4 WFMD Products

The scientific TROPOMI XCH_4 retrieval product is produced at the University of Bremen in Germany. The product provides XCH_4 retrieved from TROPOMI radiance measurements using weighting function modified differential optical absorption spectroscopy (WFMD or WFM-DOAS) retrieval method. The method is designed for a simultaneous retrieval of XCH_4 and column-averaged dry-air mole fraction of carbon monoxide, XCO [34,35]. WFMD is a linear least-squares method based on scaling (or shifting) pre-selected atmospheric vertical profiles. The vertical columns of the desired gases are determined from the measured sun-normalized radiance by fitting a linearized radiative transfer forward model to it. To enable a fast retrieval, a look-up table scheme for the radiances and their derivatives has been implemented, containing various reference spectra characterizing a variety of typical atmospheric conditions, covering combinations of different solar zenith angles, altitudes, albedos, water vapor contents, and temperatures. The reference spectra are computed with high spectral resolution in line-by-line mode and are subsequently convolved to the TROPOMI spectral resolution of the shortwave infrared wavelength bands. The linearized radiative transfer model, plus a low-degree polynomial, are linear least squares-fitted to the logarithm of the measured sun-normalized radiance. The trace gas vertical profiles (CH_4, CO, and H_2O) are scaled for the fit (i.e., the profile shape is not varied from the a priori profile). Additional fit parameters are the shift of a pre-selected temperature profile, a scaling factor for the pressure profile, and parameters for a polynomial of the second order (original settings) or third order (since v1.8; [35]).

Information on potential cloud contamination is obtained from strong H_2O absorption lines in the TROPOMI spectral band 8 by comparing the measured radiances to reference radiances for cloud-free conditions. In the retrieval post-processing, the retrieved vertical columns are converted to column-averaged dry-air mole fractions by dividing them by the dry-air columns obtained from the European Centre for Medium-Range Weather Forecasts (ECMWF) data. To adopt the high spatial resolution of the TROPOMI data, the ECMWF dry-air columns are adjusted for the actual elevation of the individual satellite scenes by accounting for the mismatch to the mean altitude of the coarser model grid.

As the look-up table is confined to specific atmospheric conditions, such as cloud-free scenes, an efficient machine learning quality filtering procedure based on a random forest classifier is trained using quasi-simultaneous cloud information from VIIRS. After the supervised learning process has been completed, the ongoing actual quality prediction of individual soundings is independent of the VIIRS data. Due to the strict quality requirements for retrieving atmospheric methane, a shallow learning random forest regressor is trained to reduce the remaining systematic coarse-scaled methane dependencies on other parameters such as albedo after quality filtering. The training is restricted to a subperiod of time and a few small regions, which are selected to cover the entire range of albedo values and all possible viewing geometries. Starting with v1.8, post-processing also includes an efficient orbit-wise destriping filter based on combined wavelet–Fourier filtering to remove stripes in flight direction in the TROPOMI XCH_4 and XCO data, while optimally preserving the original spatial trace gas features [35]. In this work, two WFMD data product versions were used: v1.2 and v1.8. The latter was the newest version at the time of writing of this paper.

2.3. TCCON Sites and XCH_4 Products

The Total Carbon Column Observing Network (TCCON) is the main validation network for greenhouse gas observations from space [43,44]. TCCON is a network of

ground-based high-resolution Fourier Transform Spectrometers (FTSs) that measure direct sunlight in the near-infrared spectral region. The column-averaged dry-air mole fractions of greenhouse gases and other atmospheric trace gases (CO_2, CH_4, N_2O, HF, CO, H_2O, and HDO) are retrieved from the measured spectra. The TCCON GGG software iteratively scales an a priori trace gas profile until it finds the best fit between the observed spectrum and a forward model simulated spectrum. In the most recent major version update, the TCCON GGG2014 was updated to GGG2020. The GGG2020 version update is described in full by Laughner et al. [45]; the largest changes include improved prior trace gas profiles through a new algorithm [46], updated spectroscopy, changes in meteorological data, an updated retrieval vertical grid, improvements to the interferogram to spectrum conversion, and updated quality control.

Currently, TCCON consists of 28 operational sites, from which 23 are in the Northern Hemisphere. In this study, the focus is on the four northernmost, non-urban TCCON sites that are located to the north of 50°N and are either within or relatively close to the permafrost regions (Figure 1). In what follows, the sites are described in more detail.

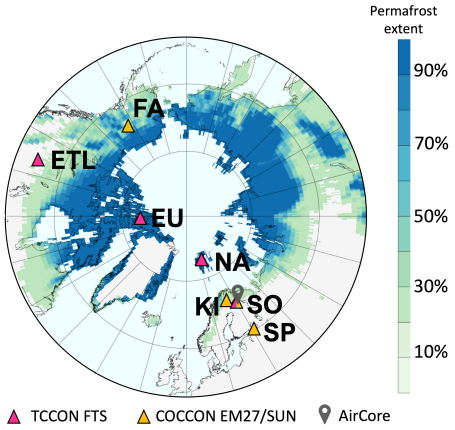

Figure 1. Locations of the high-latitude TCCON, COCCON, and AirCore sites overlaid on a map of the regional permafrost extent re-gridded from ESA CCI Permafrost data. Regions with >90% permafrost extent are considered continuous permafrost.

The TCCON station at East Trout Lake (ETL), Saskatchewan is located within the Canadian boreal forest at 54.3537°N, 104.9867°W, and 501.8 m above sea level. The nearest city is located more than 150 km away. The TCCON station is housed in an Environment and Climate Change Canada (ECCC) laboratory, which is equipped with a 60 m tall tower collecting in situ measurements of various trace gases (including CO_2 and CH_4), and a suite of surface-level aerosol measurements. The ETL TCCON spectra cover the 1800–11,000 cm^{-1} spectral range across indium antimonide (InSb) and indium gallium arsenide (InGaAs) detectors. Both GGG2014 [47] and GGG2020 [48] data versions are available.

The TCCON Sodankylä (SO) site is located in Northern Finland at 67.3668°N, 26.6319°E, at the Finnish Meteorological Institute's Arctic Space Centre. The Centre is situated about 6 km south of Sodankylä town (about 4900 inhabitants). Surroundings are predominantly a coniferous forest but there is also a peatland area nearby. In addition to TCCON, the site also contributes greenhouse gas measurements to other networks (e.g., COCCON and ICOS), and there are multiple measurements set up to monitor the atmosphere, cryosphere, hydrological phenomena, and the biosphere, enabling multidisciplinary studies. Regular measurements are taken with a Bruker 125HR FTS instrument [49]. The FTS at Sodankylä is equipped with indium gallium arsenide (InGaAs, covering 4000–11,000 cm^{-1}), a silicon diode (Si, covering 9000–15,000 cm^{-1}) and indium antimonide (InSb, covering 1800–6000 cm^{-1}) detectors. Both GGG2014 [50] and GGG2020 [51] data versions are available.

The Ny-Ålesund (NA) site in Svalbard (Norway) (78.9°N, 11.9°E) is hosted at the joint French–German research station AWIPEV. The TCCON FTIR spectrometer, a Bruker IFS120HR, which was updated to an IFS120-5HR in 2012, performs alternating measure-

ments for the TCCON and NDACC networks and is installed in the AWIPEV observatory at 20 masl. The AWIPEV station hosts a large number of atmospheric research instruments, including daily radiosondes and various meteorological quantities. The station is housed on the outskirts of Ny-Ålesund on the coast of Kongsfjorden. The surface pressure data used in the retrieval is taken from the neighboring Baseline Surface Radiation Network (BSRN: [52]). In its TCCON configuration, the measurements are performed using a CaF_2 beamsplitter and a room-temperature InGaAs diode detector. There are no solar absorption measurements performed during the polar night from October to March. Data are available in two versions: the previous GGG1014 (GGG2014: [53]) and current GGG2020 (GGG2020: [54]) releases.

The Eureka (EU) TCCON site is located on Ellesmere Island in Nunavut, Canada at 80.05°N, 86.42°W, at the Polar Environment Atmospheric Research Laboratory (PEARL, [55]). The TCCON FTIR spectrometer is installed in the PEARL Ridge Lab, at an elevation of 610 m, 15 km from the Environment and Climate Change Canada Eureka Weather Station. The facility is on the shores of Slidre Fiord and the area is semi-arid and underlaid by permafrost. There is no local community. PEARL houses about two dozen instruments for atmospheric measurements, with data contributed to multiple networks, including the Network for Detection of Atmospheric Composition Change (NDACC), AERONET, MPLNET, and the Pandonia Global Network. A Bruker 125HR FTIR spectrometer was installed in 2006 as a mid-infrared NDACC instrument [56], with near-infrared capability added in 2010; since then, measurements have alternated between TCCON and NDACC. The TCCON measurements are recorded with a CaF2 beamsplitter and an InGaAs detector. No solar measurements are possible during the four months of polar night from late October to late February, and measurements have been limited since July 2020 due to restrictions on site access. Both GGG2014 [57] and GGG2020 [58] data versions are available.

2.4. COCCON XCH_4 Product

The Collaborative Carbon Column Observing Network (COCCON) is a network of portable EM27/SUN Fourier Transform Spectrometers [59]. The spectrometer measures direct solar radiation covering spectral range of 5500–11,000 cm^{-1} with a single-detector set-up [60] and additional 4000–5500 cm^{-1} with the dual-detector set-up [61]. The spectral resolution of the instrument is 0.5 cm^{-1}. Column mixing ratios of CO_2, CH_4, H_2O, and CO are retrieved from the spectra using PROFFAST v1.0 retrieval code (available at https://www.imk-asf.kit.edu/english/4266.php, last accessed on 9 August 2024) that employs a prior profile-scaling method for spectral fitting [62].

The EM27/SUN instruments are characterized by the instrument line shape (ILS) and calibrated against the reference EM27/SUN (SN37) and the collocated Karlsruhe TCCON instrument by the Karlsruhe Institute of Technology (KIT) [63]. In an intercomparison campaign at the Finnish Meteorological Institute's Sodankylä facility, an EM27/SUN was found to have a bias and standard deviation of 0 ± 4 ppb in comparison to the Sodankylä TCCON instrument [62]. The EM27/SUN spectrometers have been found stable over timescales of several years and, due to the construction of the interferometer, do not require a lot of maintenance [63].

As with TCCON, we concentrated on the northernmost COCCON sites, which are Kiruna (KI), Sodankylä (SO), Fairbanks (FA), and St. Petersburg (SP; see Figure 1).

COCCON observations in Kiruna (KI, Sweden; [64]) are performed at the NDACC FTIR site and operated by KIT in cooperation with IRF. The observations have been used for detecting greenhouse gas gradients along the baseline Kiruna–Sodankylä [65].

The COCCON Sodankylä (SO) station is the same as the TCCON site at the FMI Arctic Space Centre (site description in Section 2.3). The EM27/SUN measurements at Sodankylä started in March 2017 during the Fiducial Reference Measurements for Greenhouse Gases (FRM4GHG) project, using an instrument from Karlsruhe Institute of Technology (KIT) with the serial number SN039 [66]. The time series was continued with another instrument (SN122)

for which data are available from April 2020 until end of March 2021 [67]. The two Sodankylä datasets were analyzed separately, and referred to by the instruments' serial numbers.

The Fairbanks (FA) COCCON station [68] is located in the interior of the State of Alaska, USA, at 64.859379°N, −147.849944°E and 222.5 m above mean sea level. The station is on the roof of the University of Alaska Fairbanks (UAF) Geophysical Institute and is on the western edge of the the small city of Fairbanks, Alaska, which has a city population of approximately 32,000 inhabitants and a broader regional population of approximately 100,000 people. The site is in forested hills, which generally cover most land around the site; however, to the south of Fairbanks there is a large flat basin filled with wetlands that has many lakes, which formed due to the poor drainage of frozen soils. Observations were made using EM27/SUN instrument SN050, which is owned by KIT and operated by UAF under a cooperative agreement between these institutions.

COCCON observations in Russia (St. Petersburg (SP) and Yekaterinburg; [69]) were collected in the framework of the H2020 VERIFY project. Further details of the campaign activities are provided by Alberti et al. [70].

2.5. AirCore CH_4 Profiles

AirCore is a technique to measure profiles of atmospheric trace gases [71]. AirCore enables traceable measurements of methane and other gases from the stratosphere down to the Earth's surface. The AirCore instrument is lifted by a meteorological balloon to the stratosphere, typically up to 30–35 km of altitude. The inlet valve of the AirCore system is open during the balloon launch and the sampler is filled during payload descent. The inlet valve of the system is closed shortly after the landing of the sampler. The gas analysis is typically performed within 2–3 h after landing of the payload, using a Cavity Ring-Down Spectrometer. The AirCore measurements are traceable by the World Meteorological Organization's in situ trace gas scales.

In the European sector of the Arctic, AirCore observations have been made at FMI Sodankylä (SO), Finland, and at Esrange, near Kiruna, Sweden. Sodankylä was the first site in Europe to perform AirCore measurements. In Sodankylä, we have performed AirCore flights during various seasons since early September 2013. In the case of the AirCore measurements taken at Sodankylä, the precision and accuracy for CO_2, CH_4, and CO measurements are 0.05 ppm and 0.1 ppm, 0.5 ppb and 1 ppb, and 8 ppb and 3 ppb, respectively, [62]. For this study, we included all AirCore measurements carried out in Sodankylä in the years 2018–2021, totaling 18 flights.

2.6. Permafrost Extent

Permafrost is a layer of ground that remains at or below the freezing temperature of water for at least two consecutive years [72]. Permafrost areas consist of an active layer, which is subject to seasonal ground freezing, and perennially frozen ground beneath the active layer.

In this study, we used the ESA CCI Permafrost Year 3 Climate Research Data Package (CRDP v2) [73]. It provides annual datasets of permafrost extent, temperature, and active layer thickness. The extent data are gridded products in polar stereographic projections at 1 km resolution and based on the World Geodetic System 84 (WGS84) reference ellipsoid. As described in the CCI Permafrost extent data catalog webpage (https://dx.doi.org/10.5285/6e2091cb0c8b4106921b63cd5357c97c, last accessed on 9 August 2024), CCI Permafrost extent data are given as a yearly fraction of permafrost-underlain and permafrost-free areas within a grid cell. A classification according to the IPA (International Permafrost Association) zonation for the permafrost zones is as follows: isolated (0–10%), sporadic (10–50%), discontinuous (50–90%), and continuous permafrost (90–100%). Continuous permafrost is, as the name suggests, a uniform, continuous sheet of frozen material. Continuous permafrost is considered when 90% of the ground surface is permafrost, taking into account small taliks, patches of unfrozen ground that may exist within the continuous layer of frozen perennial ground, mainly under water bodies.

We re-gridded the original fraction to a 0.25° × 0.25° grid to speed up the co-location of TROPOMI Level 2 data over the permafrost regions. The re-gridded permafrost fraction is an average of the original fractions. These re-gridded values were then categorized according to the IPA permafrost zones described above. Since the permafrost data were only used in this study to estimate methane satellite data coverage and amounts, we chose permafrost data from the year 2017 for the analysis and did not update the dataset for each year.

3. Methods

3.1. Co-Location at TCCON and COCCON Sites

To make the ground-based and satellite-based observations spatially and temporally consistent, they have to be co-located. Every co-location technique is an assumption about the geographical region and temporal correspondence on which the observations can be assumed to measure the same atmospheric methane.

As the number of TROPOMI XCH_4 observations is sufficiently large, a simple method for spatial co-location can be used: we considered all TROPOMI observations ±2° in latitude and longitude from the TCCON and COCCON site locations. Temporally, we considered all ground-based observations within one hour of each TROPOMI overpass. In addition, to avoid spurious outliers in the analysis due to insufficient data, a minimum of three good-quality TROPOMI observations per day were required inside the co-location region, on any overpass during the day.

To compare same-day XCH_4 values, we calculated the daily median values from both TCCON and TROPOMI data for each day that had co-located observations. These daily median values were then used in the TROPOMI evaluation. For the comparison between TCCON/GGG2014 and TCCON/GGG2020 (Section 4.2.2), the temporal co-location criterion was more relaxed, allowing all same-day observations, as the prior correction (Section 3.2) was not applied in that part of the study.

3.2. Prior Correction

To account for the impact of different retrieval priors in the comparison of satellite and ground-based remote sensing products, a prior correction was applied to the TROPOMI XCH_4 observations. Following Rodgers [74] and the notations of, e.g., Schneising et al. [34], we adjusted the original TROPOMI-retrieved column-averaged dry-air mole fraction $\hat{c}$ by assuming the TCCON or COCCON prior profile $\bar{x}_{a,\mathrm{ref}}$ as the common prior profile for both retrievals. The adjusted TROPOMI retrieval result $\hat{c}_{\mathrm{adj}}$ is, thus,

$$\hat{c}_{\mathrm{adj}} = \hat{c} + \sum_l h_l (1 - A_l)(x^l_{a,\mathrm{ref}} - x^l_a), \tag{1}$$

where h_l is the pressure weighting function, A_l the TROPOMI column-averaging kernel, and x^l_a the TROPOMI prior dry-air mole fraction at an atmospheric vertical layer l.

We quantified the impact of the prior correction ($\hat{c}_{\mathrm{adj}} - \hat{c}$) against both TCCON and COCCON data. The results of the TROPOMI XCH_4 adjustment using the COCCON prior are shown in Figure 2. For OPER rpro, the COCCON prior correction impact is mostly negative, i.e., the correction leads to lower XCH_4 values. In Kiruna, the prior correction leads to up to 7.2 ppb higher XCH_4 values during spring 2019, but the impact is still mostly negative, with a minimum of −6.9 ppb in 2020. At the other COCCON sites, the correction effect varies from −5.8 ppb to 1.9 ppb. A solar zenith angle dependence can also be seen for TROPOMI OPER rpro's COCCON-prior-adjustment: the adjustment leads to larger negative values at larger solar zenith angles (∩-shaped). For WFMD v1.8, the impact of the COCCON prior adjustment is always positive, i.e., the TROPOMI XCH_4 values are corrected upwards. The adjustment is overall smaller in magnitude when compared to OPER rpro: the differences between the prior corrected and uncorrected WFDM v1.8 daily median values are less than 4 ppb. For WFMD v1.8, a solar zenith angle dependence on the impact of the prior correction can also be seen (∪ shaped).

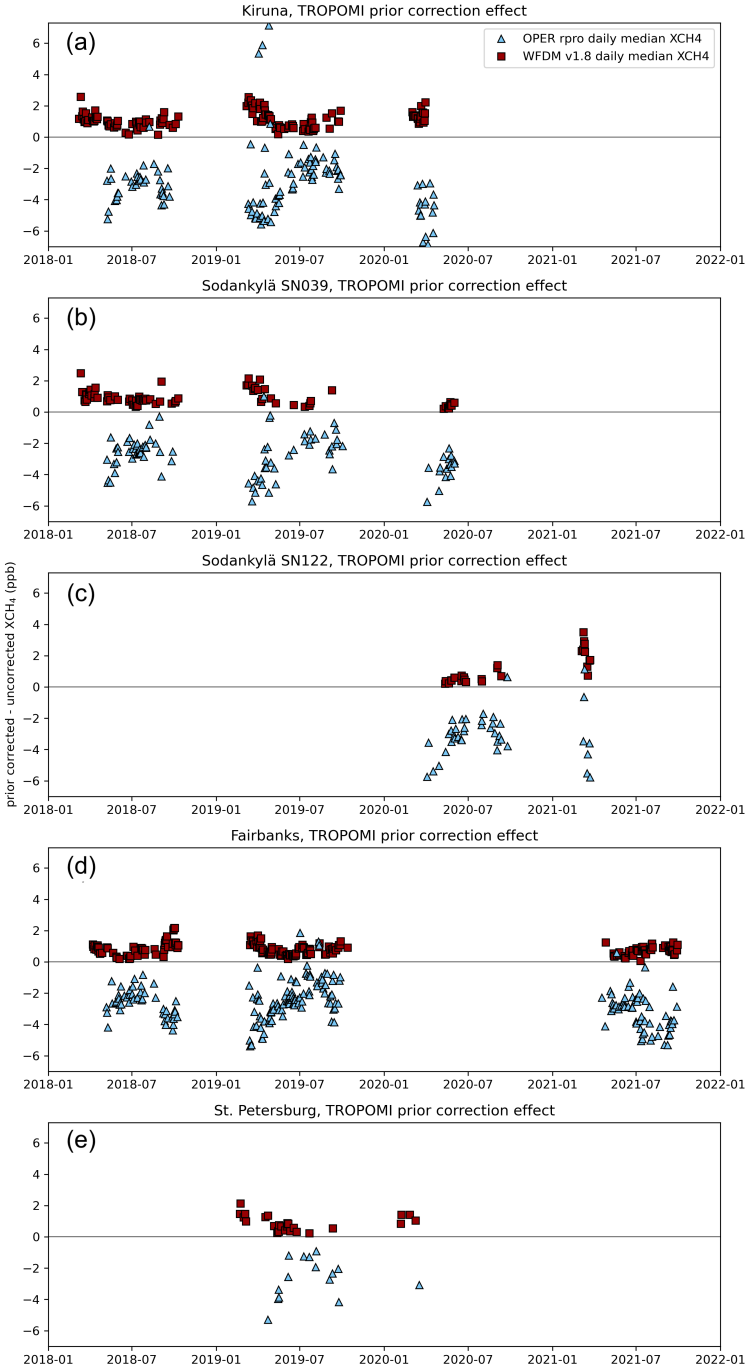

Figure 2. Effect of the COCCON prior correction on TROPOMI OPER rpro (blue) and WFMD v1.8 (red) daily median XCH_4 at (**a**) Kiruna, Sweden, (**b**) SN039 and (**c**) SN122 in Sodankylä, Finland, (**d**) Fairbanks, Alaska, USA, and (**e**) St. Petersburg, Russia.

The results of TROPOMI XCH_4 adjustment using the TCCON GGG2020 priors were different than for the COCCON: for OPER rpro, the TCCON correction was generally smaller than for WFMD v1.8, and the solar zenith angle dependence was more visible for WFMD v1.8 than for OPER rpro. For both retrievals, the correction was ∪-shaped, more clearly so for WFMD v1.8. The adjustment varied from −5.7 ppb to 4.7 ppb for OPER rpro and from −16.2 ppb to 0.4 ppb for WFMD, depending on the site and time. For OPER rpro, the average correction was the largest at East Trout Lake (−1.2 ppb) and, for WFMD v1.8, at Ny-Ålesund (−4.4 ppb), i.e., the corrected values are generally smaller than non-corrected ones.

3.3. Co-Location and Analysis against AirCore Measurements

AirCore observations from 2018 to 2021 (total of 18 measured profiles) were co-located with TROPOMI observations within ±1 degree in latitude and longitude from the Sodankylä TCCON/COCCON site that also serves as the launch site for the AirCore balloon-borne measurements. Temporally, only good-quality satellite observations taken within 3 h from the profile measurement were considered. For XCH_4 comparisons, the AirCore profiles were extrapolated to the surface according to the measured values at the lowest altitude and to the top of the atmosphere following the TCCON GGG2020 prior profile shape.

We applied the AirCore profiles here primarily for XCH_4 comparisons with the TROPOMI products. The profiles can, however, also give guidance about the dependence of the XCH_4 difference on the prior profile shape. In the analyses, the prior profiles of the TROPOMI retrievals were first scaled to produce the TROPOMI-retrieved XCH_4 values, and, then, the scaled profiles were quantitatively compared to the AirCore at each layer. To investigate the difference of TROPOMI XCH_4–AirCore XCH_4 and to what extent that difference was explained by the deviations of the retrieval prior profile from the measured true atmospheric methane profile, an analysis of the profile shapes was conducted. We divided the profiles into the tropospheric and stratospheric parts at 250 hPa. Then, the difference in the CH_4 layer value was compared to AirCore measurements interpolated in the retrieval layer pressure. The integral of the difference over the troposphere or stratosphere was calculated and the correlation with the TROPOMI−AirCore XCH_4 difference was evaluated.

4. Results and Discussion

4.1. Seasonal and Regional Coverage

4.1.1. Spatial Comparison of TROPOMI Products

Ground-based validation gives, spatially, a very limited coverage of high latitudes due to the sparseness of the validation sites. To analyze spatial differences between satellite products, all quality-filtered TROPOMI XCH_4 retrievals were gridded into monthly mean values in a 0.25° longitude × 0.2° latitude grid for years 2018–2021. Example XCH_4 maps for selected months in the year 2020 are shown in Figure 3, and their difference for every month in 2020 in Figure 4. Difference maps for years 2018, 2019, and 2021 were qualitatively similar to 2020.

Monthly maps of TROPOMI OPER rpro and WFMD v1.8 (Figure 3) show that the spatial coverage of retrievals varies with seasons: in winter months (from November to February) the solar zenith angle is a limiting factor for successful retrievals at high latitudes. Between March and October, cloud cover is likely a more significant factor for filtering, as estimated by the gaps in the spatial coverage. Monthly maps of TROPOMI OPER rpro show generally similar patterns of XCH_4 as WFMD v1.8 but with somewhat sparser coverage, especially in spring months. Spatial variability in XCH_4 can be seen in all seasons for both products. In particular, XCH_4 during the springtime shows a spatial variability of about 70 ppb for a given month. In the summer, atmospheric methane is first reduced in June due to the strengthening of the atmospheric OH sink with increasing solar UV radiation. Natural sources of methane from wetlands (see, e.g., [75]) cause an increase in XCH_4 towards the late summer (July and August). The largest difference in XCH_4 is between Greenland and the continents. More subtle differences of about 30 ppb can be seen regionally.

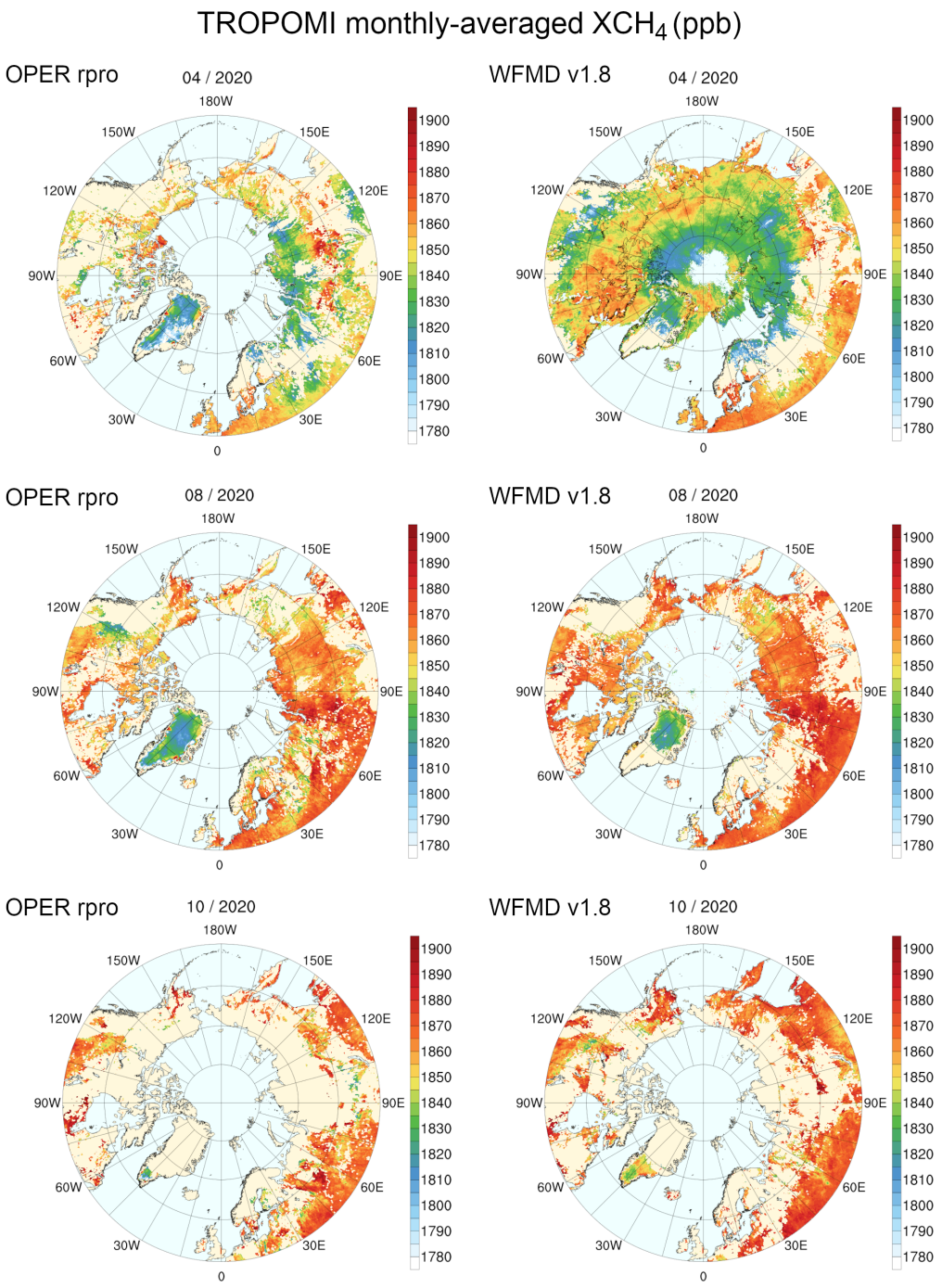

Figure 3. Spatial variability of monthly-averaged total column methane for TROPOMI OPER rpro (**left**) and WFMD v1.8 (**right**) for April, August, and October in 2020. The grid size is 0.25° × 0.2°.

The difference between TROPOMI OPER rpro and TROPOMI WFMD v1.8 monthly-averaged XCH_4 (Figure 4) changes seasonally: in the late winter and spring months, OPER rpro produces higher XCH_4 values compared to WFMD v1.8. In May, June, and September, the differences are the most negative. In July, the best agreement is achieved between the two products. Some quite localized differences of ±40 ppb can be found but, in general, the differences between the products are approximately 10 ppb in the summer months. Towards shoulder seasons, the differences increase in magnitude. The agreement between

the two products can be used as an additional measure of the reliability of spatial XCH_4 features, for instance when interpreting potential enhancements close to emissions.

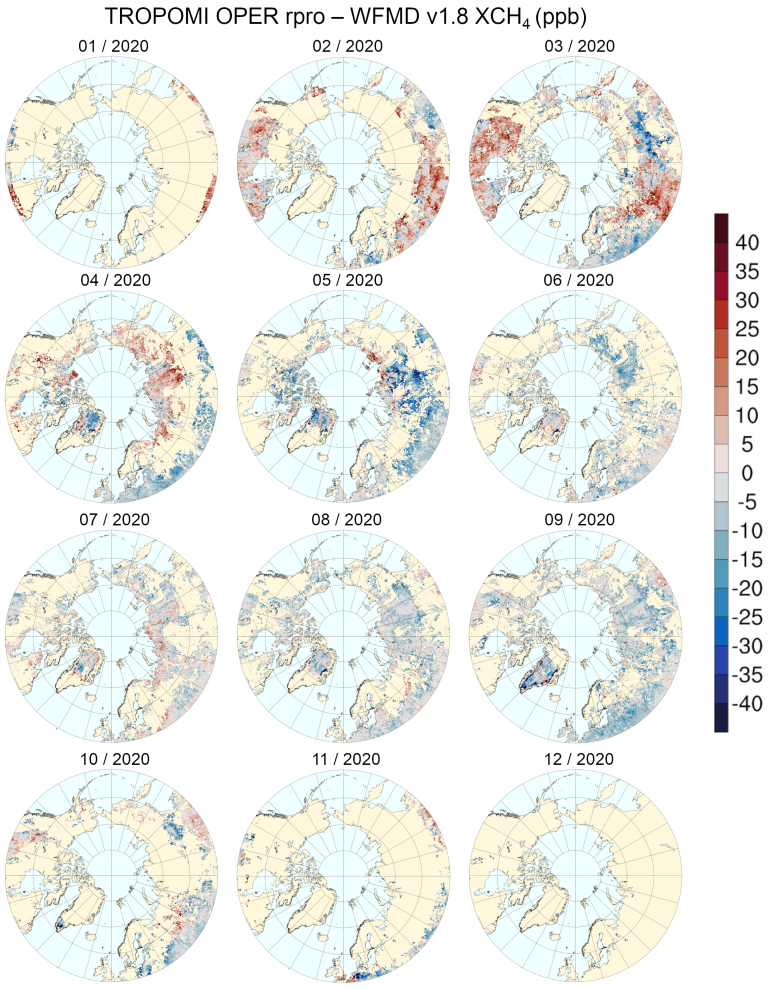

Figure 4. Spatial variability of the difference in monthly-averaged total column methane for TROPOMI OPER rpro and WFMD v1.8 in 2020. The grid size is 0.25° × 0.2°.

4.1.2. Latitudinal Comparisons

Gridded monthly mean XCH_4 values of TROPOMI methane products were further analyzed as latitudinally binned mean values. Four retrieval products (OPER, OPER rpro, WFMD v1.2, and WFMD v1.8) were considered and binned into 5° latitudinal averages. Time series of the mean differences between products are presented in Figure 5, and the temporally averaged latitudinal differences in Figure 6.

The XCH_4 difference between OPER rpro and WFMD v1.8 is mostly systematically negative; the only positive values are seen between 50°N–65°N in January–April. At the northernmost latitudes (>80°N), the differences are the most negative, averaging to about −25 ppb in August. For comparison, at 50–55°N, the difference in August varies only between −5 to −10 ppb. High positive values of the mean difference in November 2019 and 2020 are based on few soundings, interpreting from the maps in Figure 4. The temporally averaged mean difference is negative, as seen in Figure 6a, and increasingly negative towards higher latitudes.

TROPOMI retrieval product development at high latitudes can be demonstrated by comparing the current products to their earlier versions. Based on the time series in Figure 5b, TROPOMI OPER differs significantly from OPER rpro, especially at latitudes >55°N. The product differences depend on latitude as well as season. The mean difference is -9.4 ± 6.5 ppb at 55°N–60°N and increases up to 24.5 ± 3.1 ppb at the highest latitudes.

TCCON comparisons of these products (see Section 4.2) suggest product improvement in terms of reduced biases especially at the highest latitudes with the new product version, OPER rpro.

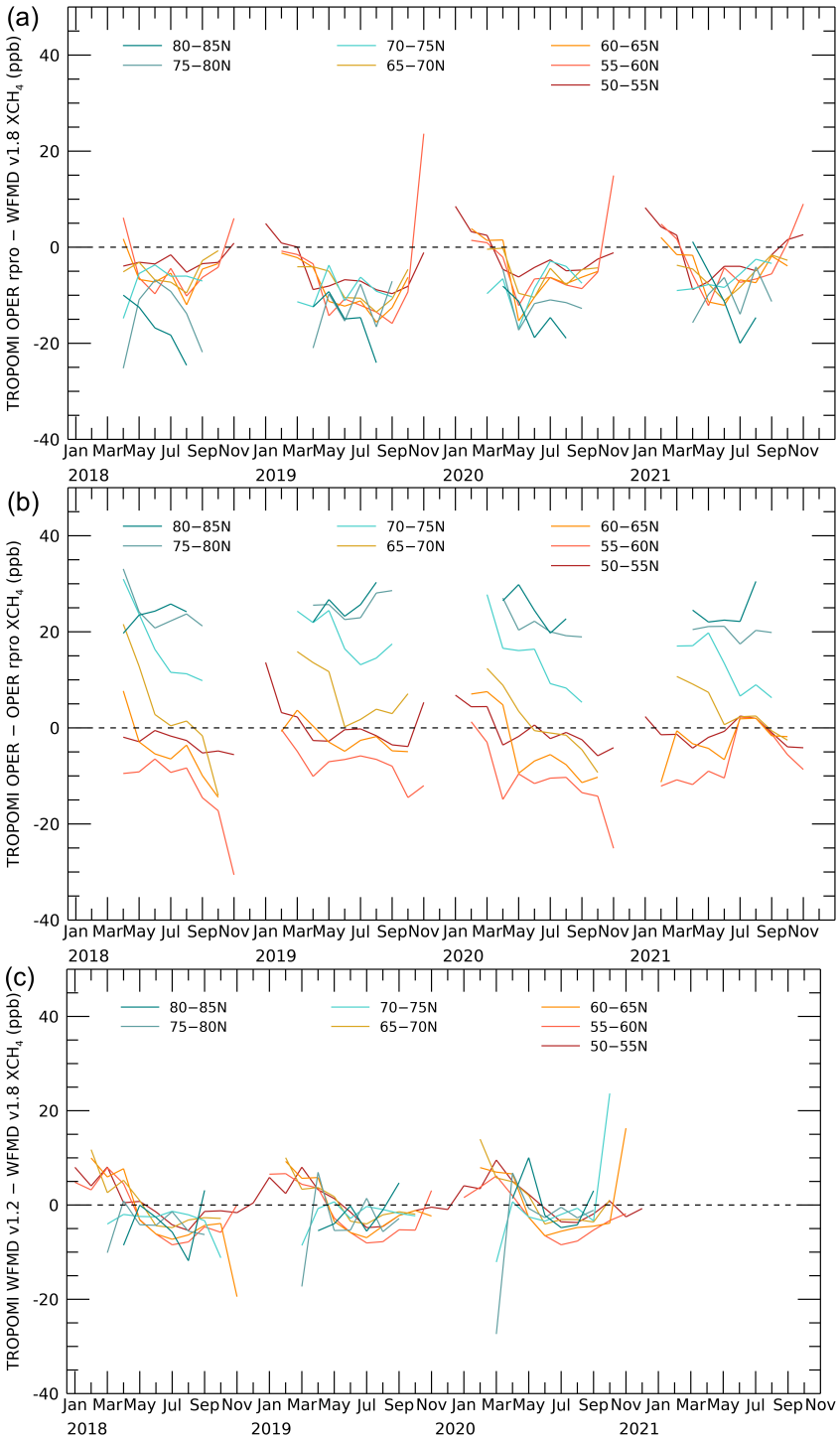

Figure 5. Temporal dependence of (**a**) TROPOMI OPER rpro–WFMD v1.8 XCH_4 difference, (**b**) TROPOMI OPER–OPER rpro XCH_4 difference, and (**c**) TROPOMI WFMD v1.2–WFMD v1.8 XCH_4 difference, colored based on 5-degree latitude bands north of 50°N. Gaps represent missing data.

Conversely, the difference between TROPOMI WFMD v1.2 and WFMD v1.8 is not as large as for OPER product versions. A modest seasonal cycle exists in the difference. While the difference shows positive values in the spring and negative values in autumn,

the temporal average (Figure 6c) is close to zero. The largest systematic difference between WFMD product versions is at the latitude band 75°N–80°N and equals -4.2 ± 7.4 ppb.

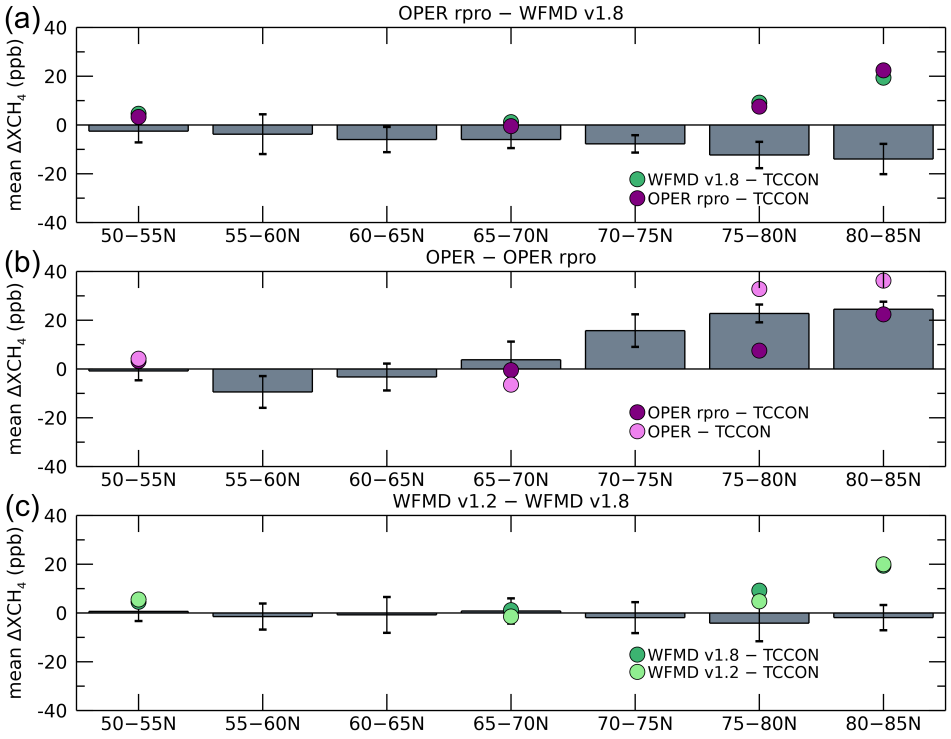

Figure 6. Averages of (**a**) TROPOMI OPER rpro–WFMD v1.8 XCH_4 difference, (**b**) TROPOMI OPER–OPER rpro XCH_4 difference, and (**c**) TROPOMI WFMD v1.2–WFMD v1.8 XCH_4 difference for different latitude bands. The error bars denote the standard deviation. Colored circles denote the mean difference of the satellite product to the ground-based TCCON instrument (GGG2020 retrieval) located in that latitude band.

4.1.3. Coverage of TROPOMI at High Latitudes

To estimate the seasonal coverage of good-quality retrievals from OPER, OPER rpro, WFMD v1.2, and WFMD v1.8, and their potential to yield information on changes in the permafrost regions, the retrievals between 2018 and 2021 (for WFMD v1.2, only 2018–2020) were classified into three categories: (1) all high-latitude retrievals north of 50°N, (2) discontinuous permafrost (permafrost extent $\in [50\%, 90\%]$), and (3) continuous permafrost (permafrost extent $> 90\%$), based on ESA Permafrost CCI Level 4 product for year 2017 (see Figure 1).

The number of observations in high latitudes is presented as a time series in Figure 7 for OPER, OPER rpro, WFMD v1.2, and WFMD v1.8. For both OPER and WFMD products, the number of retrievals has increased for the updated product versions, but the seasonal coverage has remained similar to the older product versions. The seasonal observational coverage at all regions to the north of 50°N is approximately Jan–Nov for OPER rpro and is, in principle, gapless for WFMD v1.8. Over the permafrost regions, OPER rpro retrievals cover months between Mar–Sep while WFMD v1.8 also shows a few retrievals over these regions in February and October. With the exception of OPER rpro in the year 2020, all retrieval products in Figure 7 systematically show the largest number of observations in April. This is probably caused by reduced cloud cover in April and, especially for WFMD products, the retrievals over the frozen Arctic Ocean (see Figure 3, top right) add to the total number of high-latitude observations in late winter and spring.

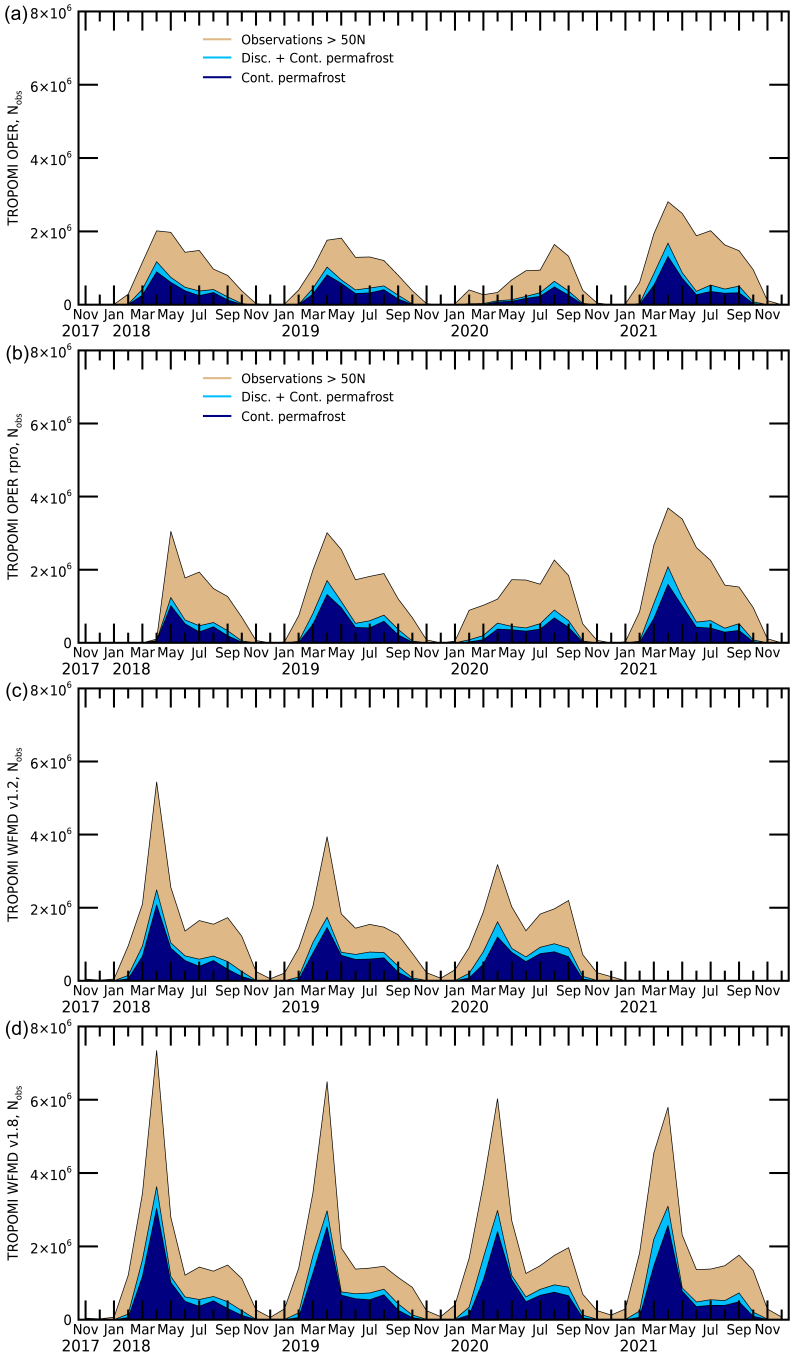

Figure 7. Seasonal dependence of the number of TROPOMI observations over different permafrost regions for (**a**) OPER, (**b**) OPER rpro, (**c**) WFMD v1.2, and (**d**) WFMD v1.8. The colors refer to different permafrost classes, determined using the ESA Permafrost CCI Level 4 product.

4.2. TROPOMI Evaluation at the TCCON Sites

Retrievals of XCH_4 from TROPOMI OPER rpro and WFMD v1.8 were evaluated at four high-latitude TCCON sites: East Trout Lake, Sodankylä, Ny-Ålesund, and Eureka. In addition to the newest satellite-retrieval products, the earlier product versions from each retrieval system (OPER and WFMD v1.2) were considered and those results are briefly discussed. Moreover, the TCCON retrieval has recently been updated from GGG2014 to GGG2020 with significant changes, e.g., improved prior profiles [46]. Both data versions of the TCCON retrievals were considered, with the emphasis on the newest data product. The comparisons cover years 2018–2021.

4.2.1. TROPOMI XCH_4 Evaluation against TCCON GGG2020

Time series of daily median XCH_4 from ground-based TCCON GGG2020, TROPOMI OPER rpro, and WFMD v1.8, and TROPOMI−TCCON XCH_4 differences are shown in Figures 8–11 for East Trout Lake, Sodankylä, Ny-Ålesund, and Eureka. Corresponding time series for earlier TROPOMI product versions OPER and WFMD v1.2 can be in from Appendix A, Figures A1–A4.

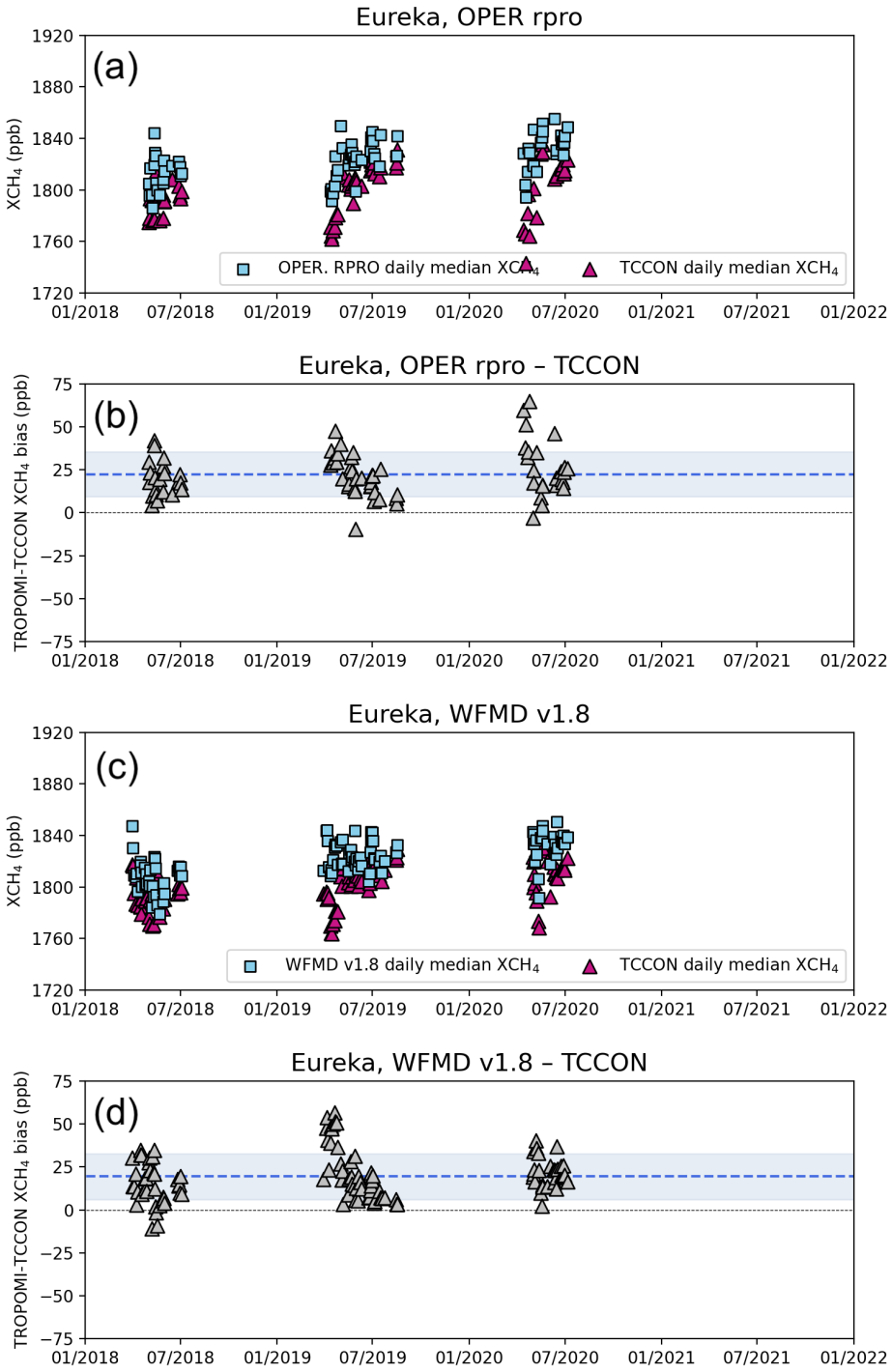

Figure 8. Daily median XCH_4 from TCCON GGG2020 (blue) and co-located TROPOMI (red) (**a**) OPER rpro and (**c**) WFMD v1.8 retrievals, and TROPOMI–TCCON differences (**b**,**d**) at Eureka, Canada. The dashed line in (**b**,**d**) shows the mean difference at the site and shaded area the standard deviation of the mean.

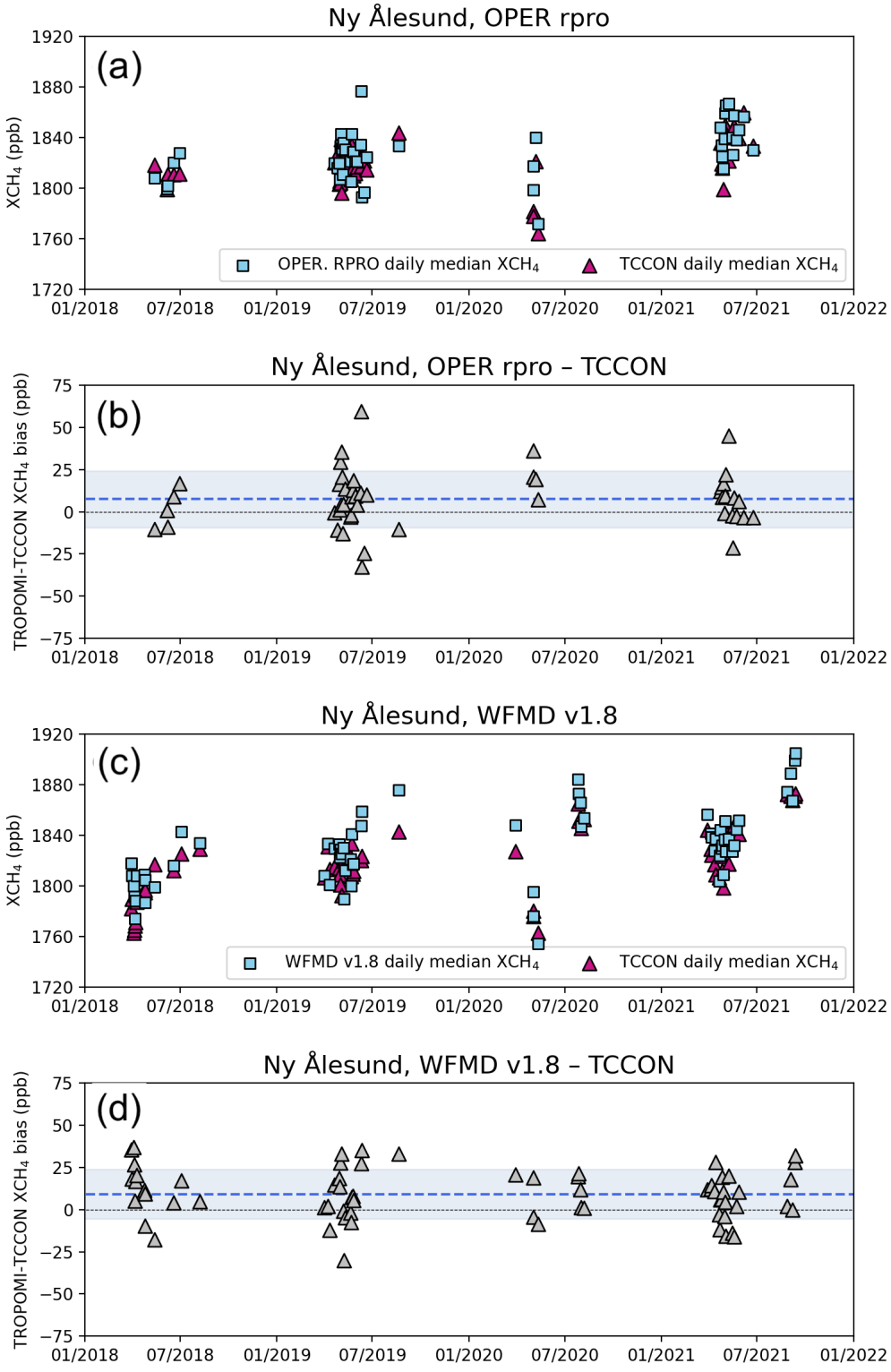

Figure 9. Daily median XCH_4 from TCCON GGG2020 (blue) and co-located TROPOMI (red) (**a**) OPER rpro and (**c**) WFMD v1.8 retrievals, and TROPOMI–TCCON differences (**b**,**d**) at Ny-Ålesund, Norway. The dashed line in (**b**,**d**) shows the mean difference at the site and shaded area the standard deviation of the mean.

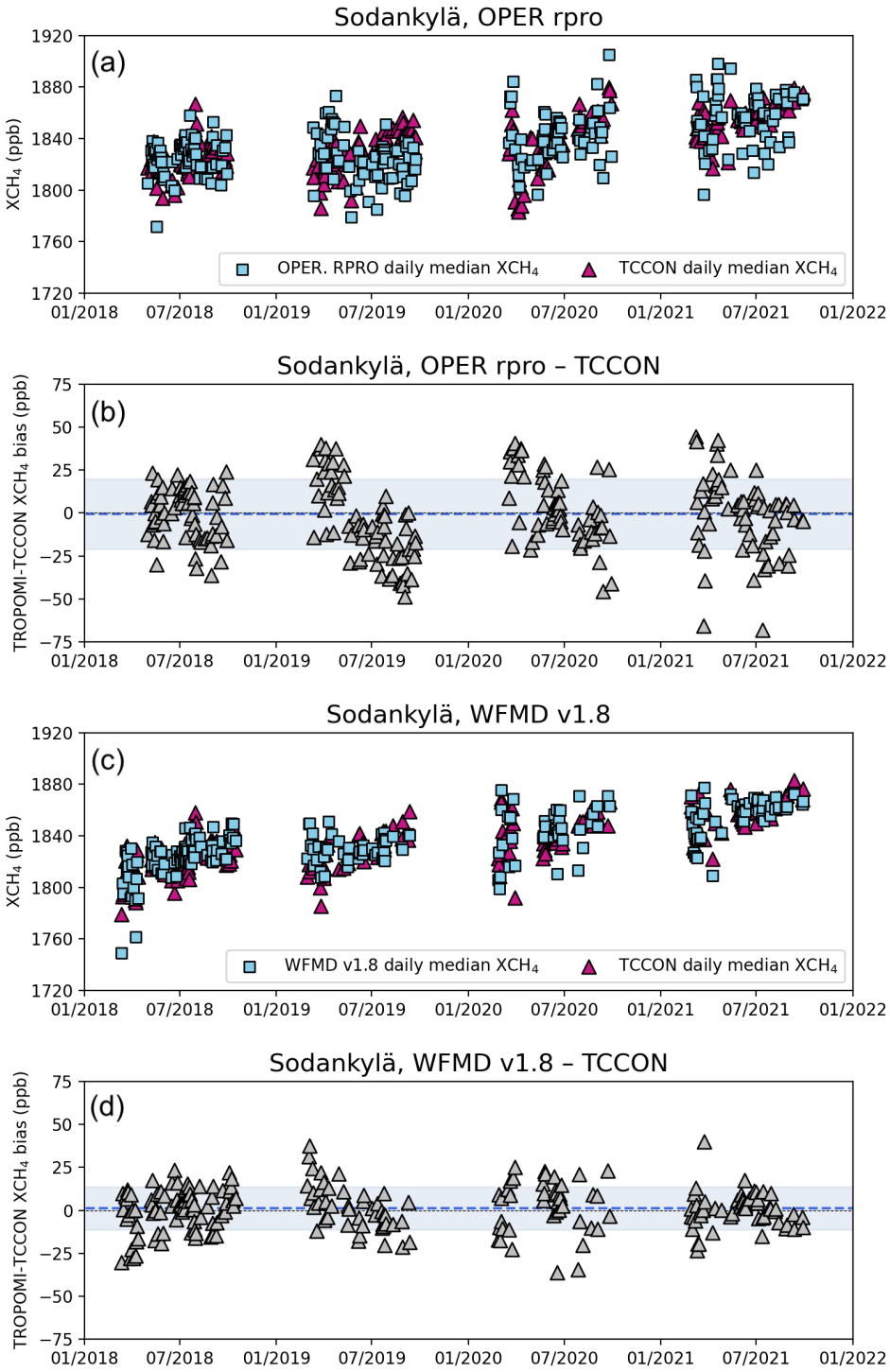

Figure 10. Daily median XCH_4 from TCCON GGG2020 (blue) and co-located TROPOMI (red) (**a**) OPER rpro and (**c**) WFMD v1.8 retrievals, and TROPOMI–TCCON differences (**b**,**d**) at Sodankylä, Finland. The dashed line in (**b**,**d**) shows the mean difference at the site and shaded area the standard deviation of the mean.

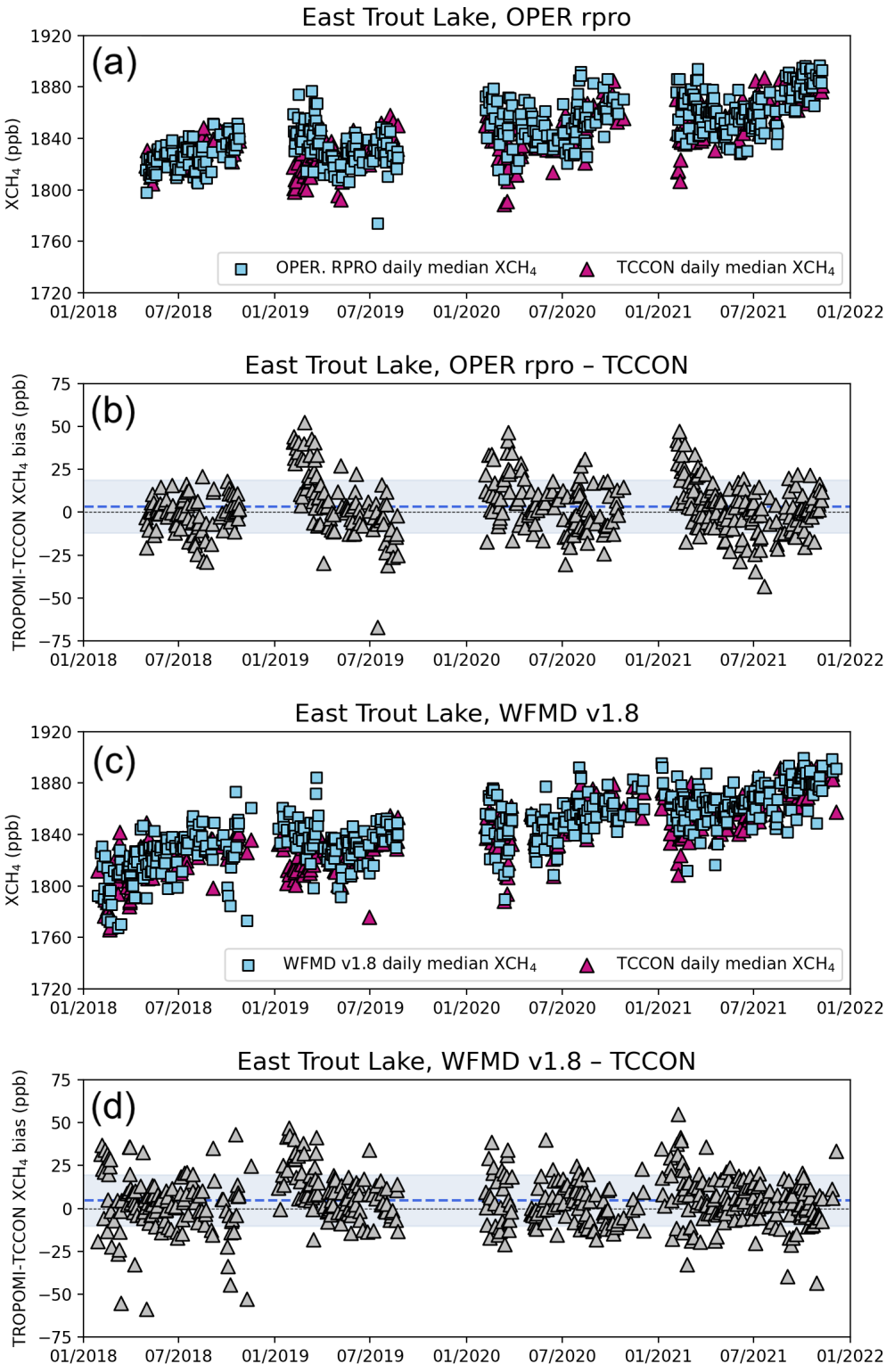

Figure 11. Daily median XCH_4 from TCCON GGG2020 (blue) and co-located TROPOMI (red) (**a**) OPER rpro and (**c**) WFMD v1.8 retrievals, and TROPOMI–TCCON differences (**b**,**d**) at East Trout Lake, Canada. The dashed line in (**b**,**d**) shows the mean difference at the site and shaded area the standard deviation of the mean.

Time series of XCH_4 and the difference indicate that the satellite products do not contain significant outliers. Both products show systematically higher values than the TCCON at Eureka, which is the northernmost site in the comparison and, therefore, the

seasonal gap in observations is extensive. In 2019, the difference with TCCON is time-dependent for both products, yielding higher values in the spring (up to about 50 ppb) and less than 10 ppb in autumn (Figure 8b,d). This seasonal dependence is also seen for the year 2020 for OPER rpro but not for WFMD v1.8. At Ny-Ålesund, the number of co-located observations is strongly limited by the vicinity of the ocean, in addition to large SZAs. The differences with TCCON are, on average, 7.5 ppb for OPER rpro and 9.2 ppb for WFMD v1.8 (Figure 9a,c). No seasonal dependence on the difference is seen, possibly due to the limited seasonal coverage. At Sodankylä, the seasonal coverage of co-located observations extends to about 7 months. The mean difference of OPER rpro with TCCON is -0.5 ± 20.4 ppb. The high scatter in the result is due to the temporal variability in the difference: OPER rpro shows a systematic, time-dependent difference with TCCON for the years 2019–2021 that exceeds 70–80 ppb, with high values in the spring and low values in autumn (Figure 10b). For WFMD v1.8, the mean difference is 1.2 ± 12.5 ppb. The seasonal variability in the difference is only present in the year 2019 (Figure 10d). At East Trout Lake, the results are qualitatively similar to those at Sodankylä but the seasonal gap in observations is shorter and is limited by the TROPOMI observations (Figure 11b,d). The mean differences for all sites are listed in Table A1.

Lorente et al. [31] showed that the mean bias of OPER rpro− TCCON/GGG2014 at 13 TCCON sites was −3.4 ppb and the mean standard deviation of the differences was 12.7 ppb. The mean bias is in the same order of magnitude as our results and the standard deviation is smaller due to averaging over global TCCON stations. They also pointed out a similar seasonal bias at high-latitude stations, and noted that the bias was positive during spring months and negative in autumn. Lorente et al. [31] suggested that the seasonal dependence of the bias is mainly caused by retrieval errors related to snow and meteorological dynamics rather than sampling errors or different priors.

The Pearson correlation coefficients between TROPOMI and TCCON XCH_4 vary for OPER rpro from 0.415 at Sodankylä to 0.761 at Eureka, and for WFMD v1.8 from 0.643 at Eureka to 0.847 at Ny-Ålesund (Table A1). At East Trout Lake, Sodankylä, and Ny-Ålesund, the correlation is higher for WFMD v1.8 than for OPER rpro, while at Eureka, the correlation is higher for OPER rpro. The largest difference in the correlations are at Ny-Ålesund where the correlations are 0.494 and 0.847 for OPER rpro and WFMD v1.8, respectively.

4.2.2. Comparison of TCCON GGG2014 and TCCON GGG2020

Because the TCCON can be considered as the primary validation resource for greenhouse gas satellite products, it is informative to quantify how the TROPOMI evaluation results have changed with the introduction of the new TCCON GGG2020 retrieval. Therefore, TROPOMI comparisons against both TCCON GGG2014 and GGG2020 were made, considering only the days that had good-quality TCCON data in both processing versions, so that potential temporal sampling differences would not affect the results. Mean differences and standard deviations of the daily median XCH_4 values are presented in Figure 12 for all high-latitude TCCON sites. The mean difference between both TROPOMI products (OPER rpro and WFMD v1.8) and TCCON becomes systematically more positive with the new TCCON data version—it seems that the high-latitude TCCON XCH_4 values have decreased by about 7 ppb on average between old and new product versions, even more at Eureka, consistent with the results in Mostafavi Pak et al. [76]. Overall, with the newest TCCON data product, the difference between TROPOMI and TCCON results is larger positive values at Ny-Ålesund and Eureka for both TROPOMI products and at East Trout Lake for WFMD v1.8. The scatter increased for both TROPOMI products at most sites, with the exception of OPER rpro at Eureka. It should be noted that the TROPOMI products do not directly apply the TCCON data for post-processing bias correction; therefore, the TROPOMI data products are independent of the ground-based data and their product versions. In addition, for this comparison, we did not apply the prior correction to the TROPOMI data as the priors have been changed between GGG2014 and GGG2020. The statistics of the comparisons are listed in Appendix B in Table A2.

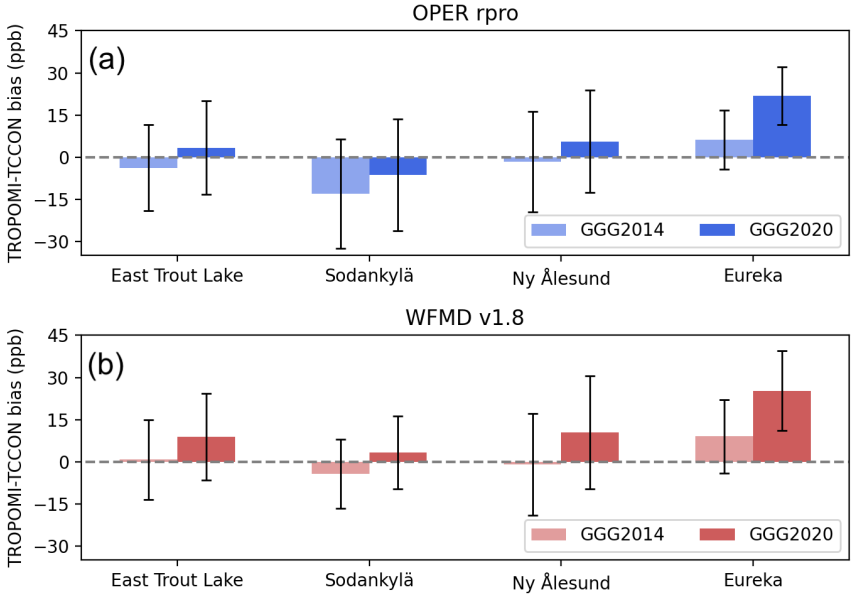

Figure 12. Comparison of TROPOMI–TCCON mean XCH_4 differences for TCCON GGG2014 and TCCON GGG2020, considering TROPOMI (**a**) OPER rpro and (**b**) WFMD v1.8 products. The TCCON data have been selected to include only the days for which both processing versions yield good-quality retrievals, so their temporal sampling is identical.

The difference of 0.35% between the TCCON data versions might result from the updated WMO scaling: for the scaling of the GGG2020 product, the number of available atmospheric profile measurements both from aircraft and AirCore measurements was increased almost two-fold compared to the previous scaling. In addition, sites with new profile measurements (e.g., Sodankylä) were included in the scaling. Improvements made in the TCCON XCH_4 retrieval may also contribute to explaining the difference. These improvements include the shape of the prior profiles, improved spectroscopy (by using a quadratic speed-dependent Voigt (qSDV) line shape with full line mixing), and improved air mass dependence removal methodology.

4.3. Evaluation at the COCCON Sites

The TROPOMI–COCCON comparisons were carried out at four high-latitude COCCON sites: Kiruna, Sodankylä, Fairbanks, and St. Petersburg. Most data for the comparisons were available at Fairbanks, totaling 205 (OPER rpro) and 188 (WFMD v1.8) days, for the period 2018–2021. Data from Kiruna and Sodankylä SN039 were available from 2018 to 2020, from Sodankylä SN122 from 2020 to 2021, and from St. Petersburg from 2019 to 2020.

The differences between daily median TROPOMI and COCCON XCH_4 for the TROPOMI OPER rpro and WFMD v1.8 products are shown in Figures 13–17. For detailed comparison values, see Table A3. Among the selected sites, Fairbanks is the only site where TROPOMI OPER rpro has a positive bias when compared against COCCON, with an average of 5.62 ppb. It also has the largest TROPOMI WFMD v1.8 average bias, 17.23 ppb, which makes it the only station at which WFMD performs worse than the OPER rpro product. For OPER rpro, the two Sodankylä sites have similar values of the difference, −6.74 ppb and −6.32 ppb at SN039 and SN122, respectively. Sodankylä SN039 also has the smallest difference for the WFMD v1.8, with an average of −0.03 ppb. The standard deviations range around 14 to 16 ppb for the OPER rpro product, with the exception of St. Petersburg, where the small amount of data likely leads to both high bias (−26.51 ppb) and standard deviation (28.73 ppb). However, this lack of data at St. Petersburg does not result in significantly different results in the WFMD v1.8 product compared to the other sites. The WFMD v1.8 standard deviations at all sites range from 11 to 13 ppb.

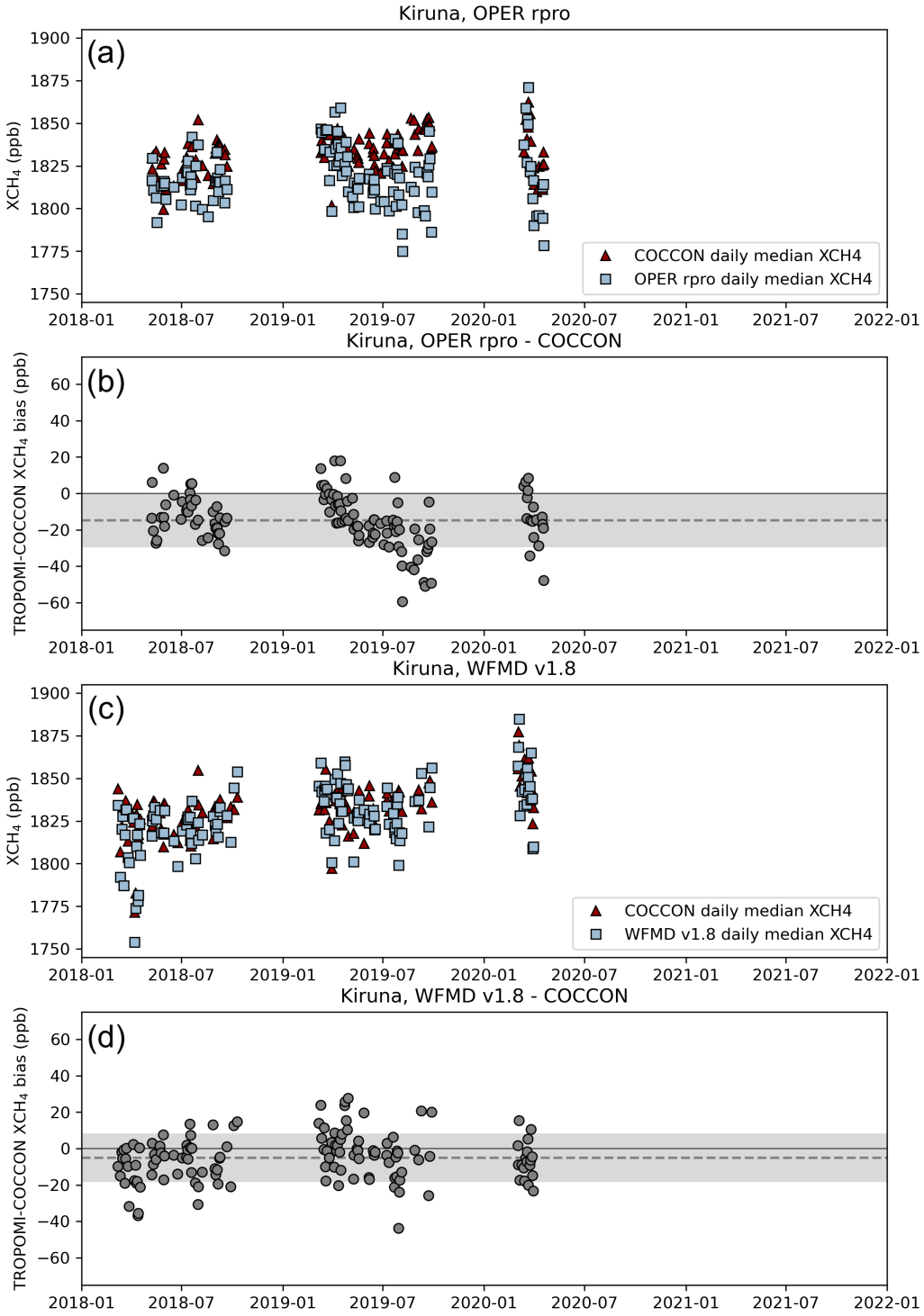

Figure 13. Daily median XCH_4 from COCCON (red) and co-located TROPOMI (blue) (**a**) OPER rpro and (**c**) WFMD v1.8 retrievals, and TROPOMI–COCCON differences (**b**,**d**) at Kiruna, Sweden. The dashed line in (**b**,**d**) shows the mean differences and the shaded area denotes one standard deviation from the mean.

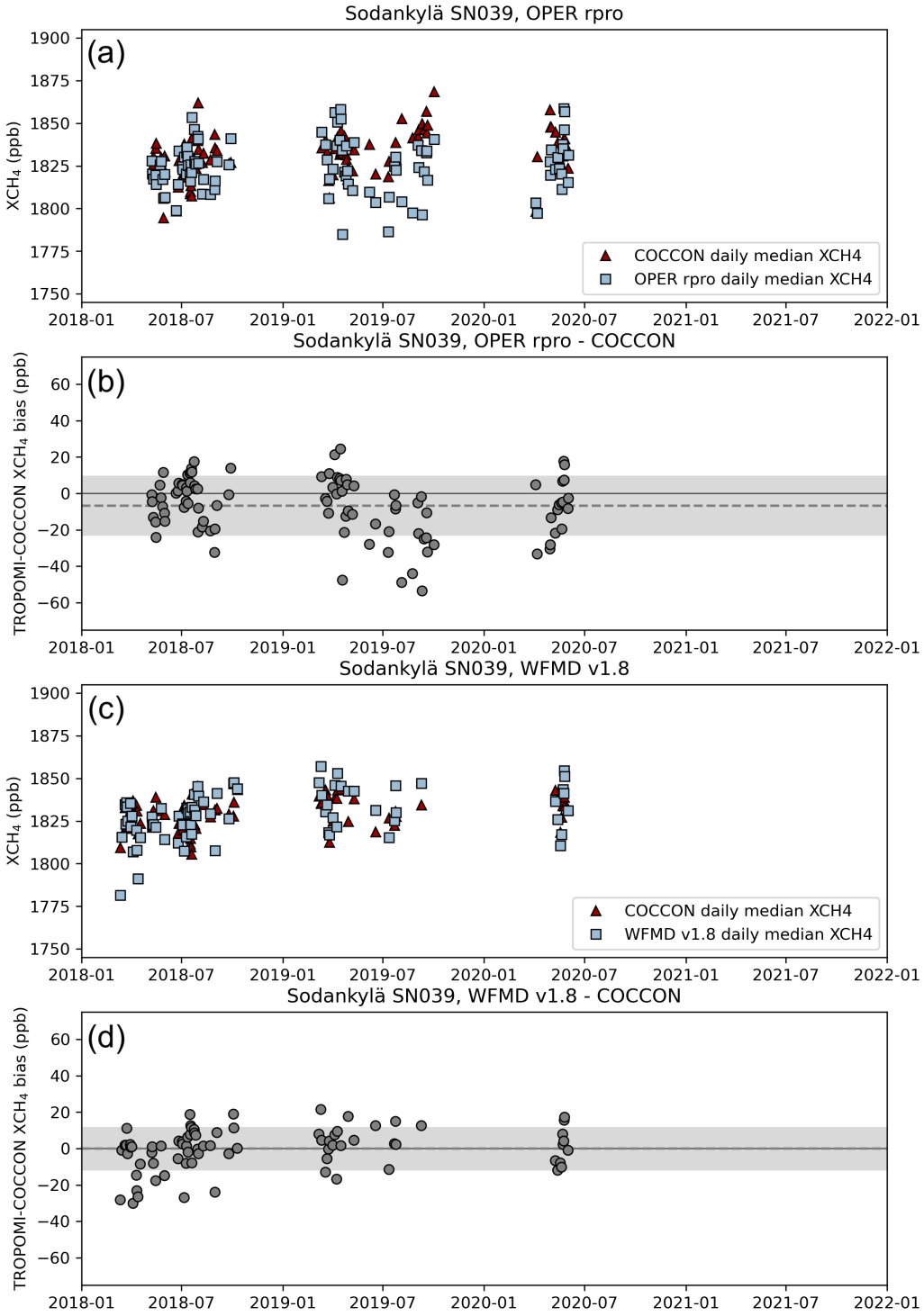

Figure 14. Daily median XCH_4 from COCCON (red) and co-located TROPOMI (blue) (**a**) OPER rpro and (**c**) WFMD v1.8 retrievals, and TROPOMI–COCCON differences (**b**,**d**) at Sodankylä, Finland (SN039). The dashed line in (**b**,**d**) shows the mean differences and the shaded area denotes one standard deviation from the mean.

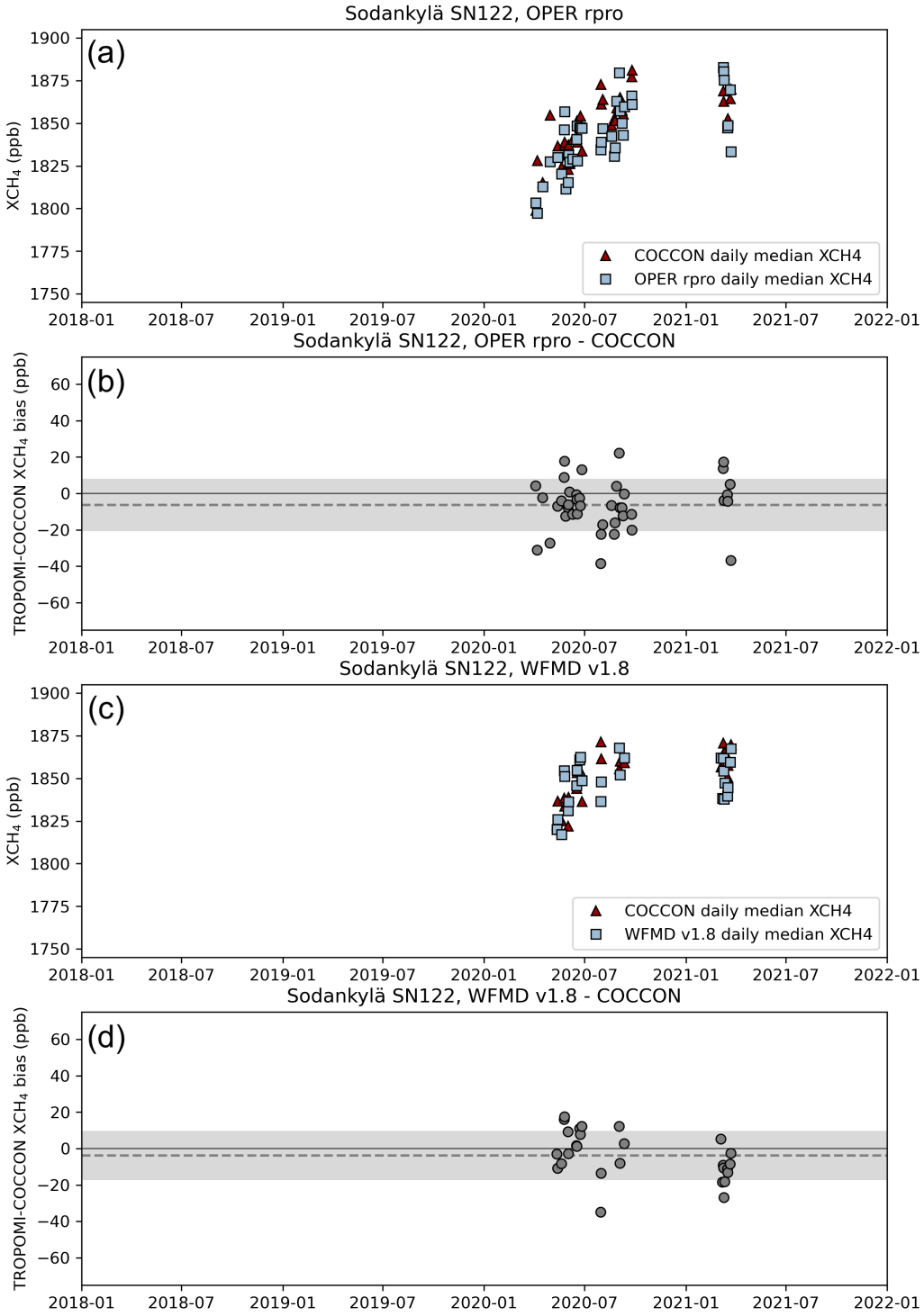

Figure 15. Daily median XCH_4 from COCCON (red) and co-located TROPOMI (blue) (**a**) OPER rpro and (**c**) WFMD v1.8 retrievals, and TROPOMI–COCCON differences (**b**,**d**) at Sodankylä, Finland (SN122). The dashed line in (**b**,**d**) shows the mean differences and the shaded area denotes one standard deviation from the mean.

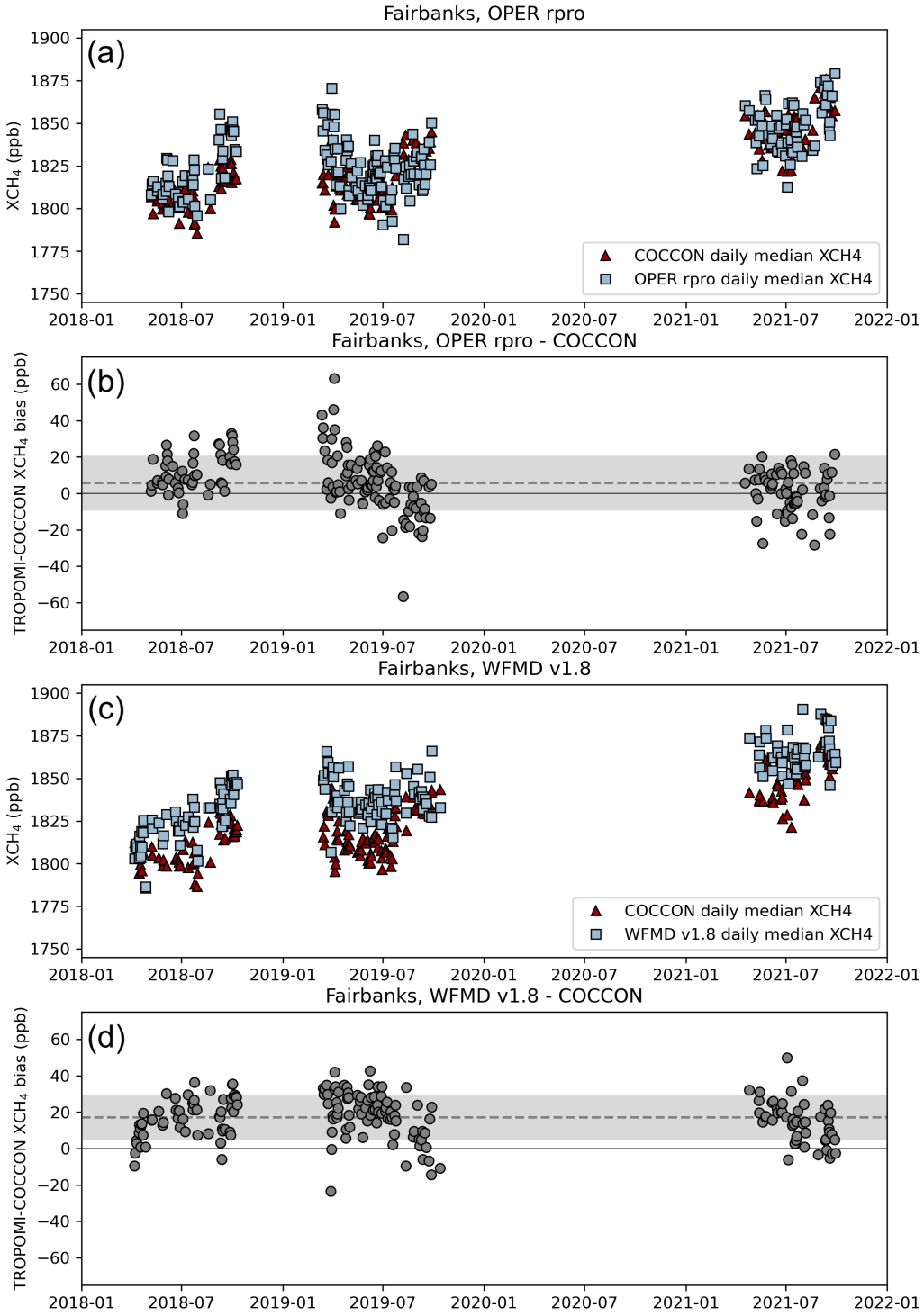

Figure 16. Daily median XCH_4 from COCCON (green) and co-located TROPOMI (orange) (**a**) OPER rpro and (**c**) WFMD v1.8 retrievals, and TROPOMI–COCCON differences (**b**,**d**) at Fairbanks, Alaska, USA. The dashed line in (**b**,**d**) shows the mean differences and the shaded area denotes one standard deviation from the mean.

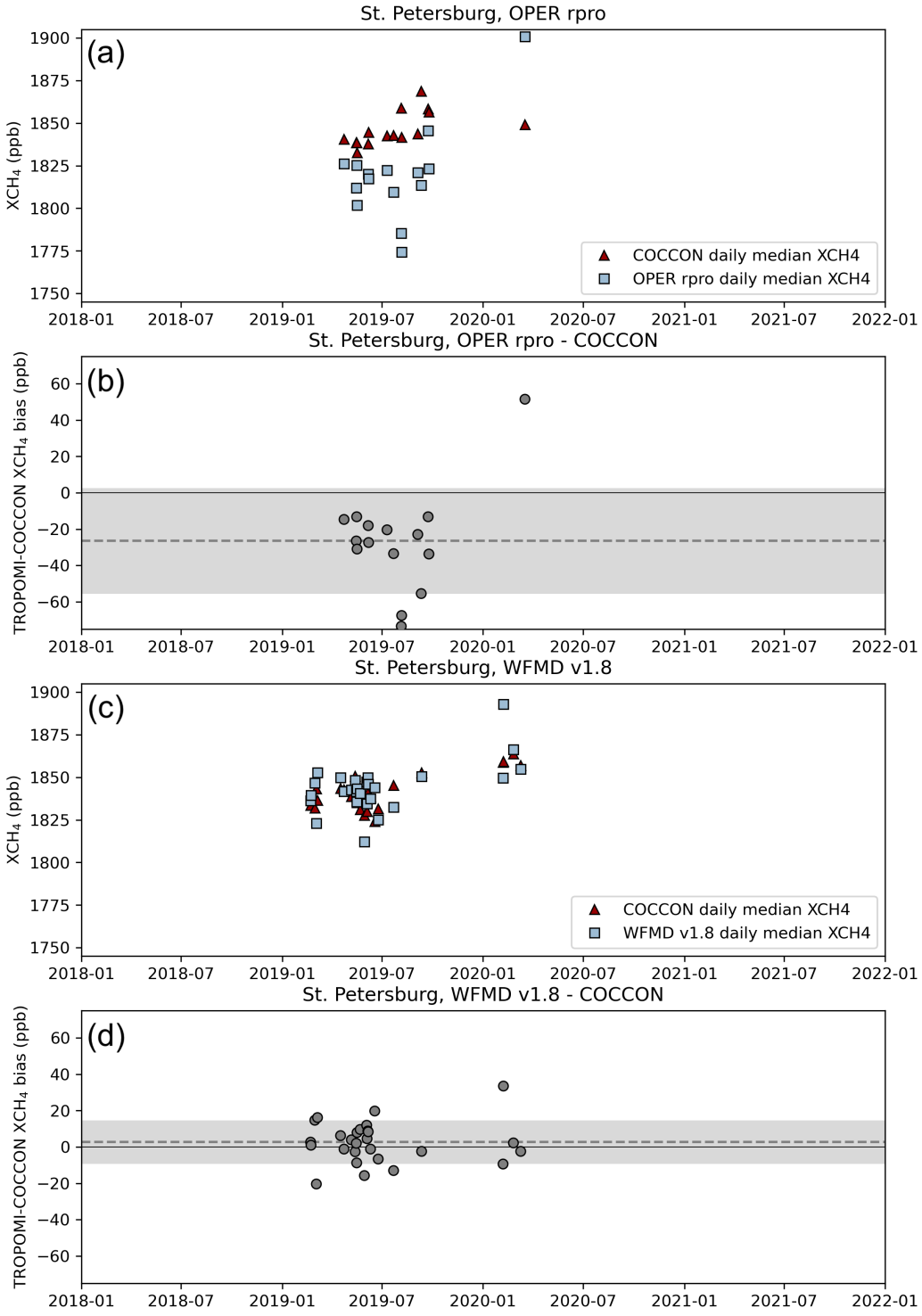

Figure 17. Daily median XCH_4 from COCCON (ref) and co-located TROPOMI (blue) (**a**) OPER rpro and (**c**) WFMD v1.8 retrievals, and TROPOMI–COCCON differences (**b**,**d**) at St. Petersburg, Russia. The dashed line in (**b**,**d**) shows the mean differences and the shaded area denotes one standard deviation from the mean.

In terms of correlations between the TROPOMI and COCCON XCH_4 observations, there are significant differences between the sites; see Table A3. The Pearson correlation coefficients range from 0.118 at St. Petersburg to 0.750 at Sodankylä SN122 for OPER rpro, and from 0.576 at Sodankylä SN039 to 0.819 at Fairbanks for WFMD v1.8. Overall, WFMD v1.8 correlates better with COCCON than the OPER rpro XCH_4, with the exception of Sodankylä SN122. Sodankylä SN122 has the highest correlation with OPER rpro, 0.750, significantly higher than SN039, 0.368, though it should be noted that SN122 has fewer than half the number of days compared to SN039. At Fairbanks, despite the high biases, both OPER rpro and WFMD v1.8 correlate well with COCCON, with Pearson correlation coefficients of 0.712 and 0.819, respectively. The temporal range of the data does not seem to be connected systematically to the correlation coefficient.

4.4. AirCore Comparisons

From 18 AirCore measurements in the years 2018–2021, the TROPOMI co-location criteria (Section 3.3) yielded eleven matching AirCore cases for OPER rpro and fpur for WFMD v1.8. An example of a measured profile along with TROPOMI OPER rpro, WFMD v1.8, and TCCON GGG2020 prior profiles is shown in Figure 18. The averages XCH_4 of all co-located TROPOMI, AirCore, and TCCON results are collected in Figure 19.

By visual inspection, TROPOMI OPER rpro prior profile shapes seem to be in a good agreement with the measured profiles. It is interesting how the scaled profile sometimes deviates more from the measurement than the prior, i.e., the scaling makes the profile agreement worse. This is particularly the case for August and September samples when TROPOMI OPER rpro yields a systematically lower XCH_4 value than AirCore or TCCON. The discrepancy of the late summer profiles is seen in the differences: TROPOMI OPER rpro scaled profiles systematically underestimate CH_4 in the troposphere in August and September, and particularly in the lowest troposphere. During that season, the measured profiles (at least in the boundary layer) could show enhancements due to local-scale emissions from nearby peatlands. In addition, in the stratosphere the prior profiles can in some situations deviate from measurements by up to −300 ppb in spring.

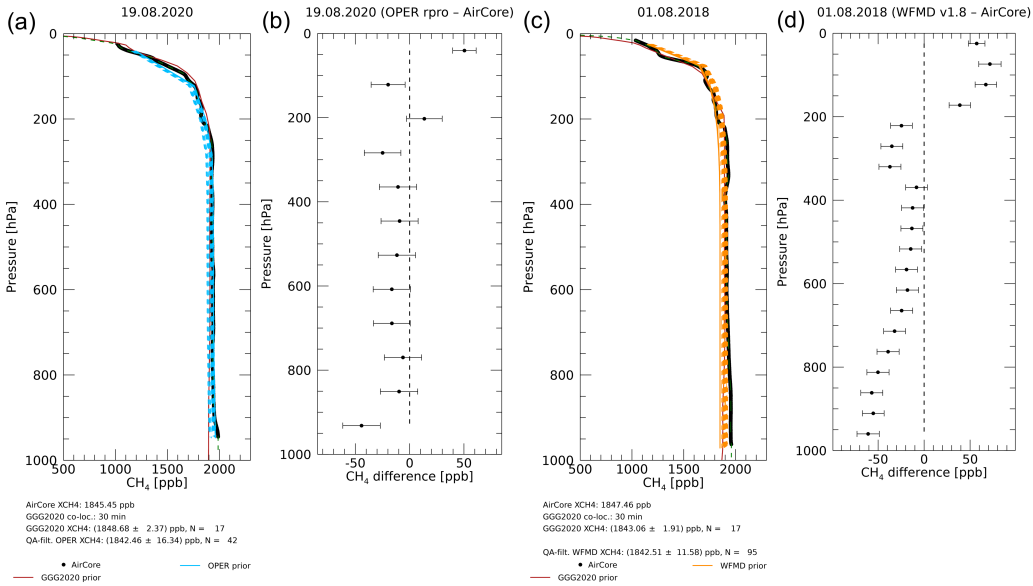

Figure 18. Comparison of measured AirCore profiles (black curves), TCCON GGG2020 prior profiles (red), and TROPOMI prior profiles: (**a**) TROPOMI OPER rpro (blue), and (**c**) TROPOMI WFMD v1.8 (orange) prior profiles. The TROPOMI prior profiles are also scaled (dashed lines) so that the profile corresponds to each retrieved XCH_4. The difference of the scaled profile compared to the measured concentration is also shown: (**b**) OPER rpro–AirCore, and (**d**) WFMD v1.8–AirCore.

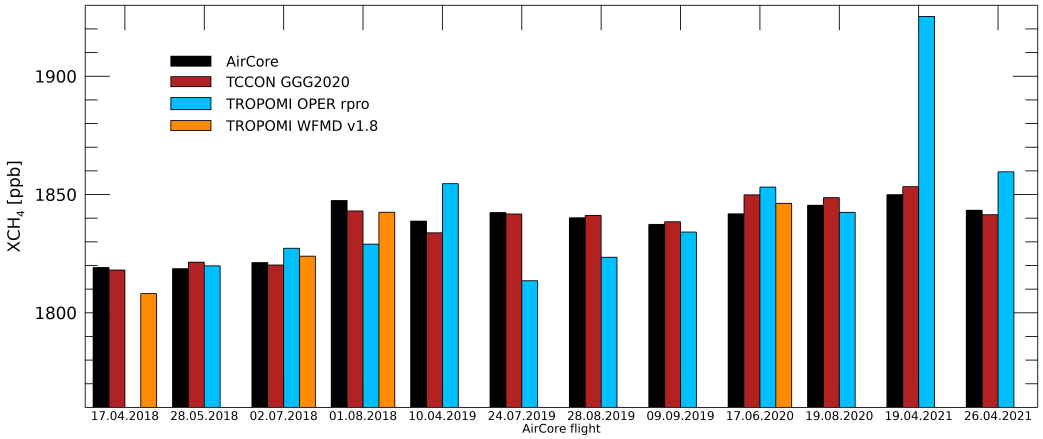

Figure 19. Collection of the AirCore XCH_4 results with co-located TCCON GGG2020 and TROPOMI observations.

The comparisons of TROPOMI WFMD v1.8 prior profiles to AirCore indicate that the WFMD prior profiles, which do not change temporally, can differ from the true atmospheric concentration profile significantly. However, the scaled profiles approach the measurement so that the retrieved XCH_4 does not deviate much from the AirCore extrapolated XCH_4 nor the TCCON GGG2020 retrieved values. The difference profiles (all qualitatively similar to Figure 18, fourth panel) show that the scaled WFMD profiles systematically underestimate CH_4 in the troposphere and overestimate in the stratosphere and, yet, the retrieved XCH_4 is close to the AirCore-extrapolated XCH_4.

It is interesting to test which part of the prior profile is more important in explaining the difference in the total column: the tropospheric or the stratospheric part. To estimate this, the individual TROPOMI prior profiles co-located with the AirCore were divided into two parts, separated at 250 hPa, and, for each pressure level of the retrieval's vertical scale, the corresponding CH_4 was interpolated from the AirCore measurement. The integrated difference through all levels of the atmosphere corresponds to the overall TROPOM–AirCore difference in XCH_4. The integrated differences were computed separately for both tropospheric and stratospheric parts, and the results were compared against the TROPOMI–AirCore difference. The results systematically indicated that the tropospheric CH_4 differences correlated better with the overall difference: for the tropospheric difference, Pearson's correlation coefficient was $R^2 = 0.90$ for OPER rpro and $R^2 = 0.86$ for WFMD v1.8, whereas, for the stratospheric difference, the results were $R^2 = 0.20$ for OPER rpro and $R^2 = 0.45$ for WFMD v1.8. A total of 1172 (OPER rpro) and 411 (WFMD v1.8) retrievals were considered. Based on the correlations, the tropospheric part is more significant in explaining the difference in the total column, even though the differences in the stratosphere could be much larger per layer. This finding is understandable considering that most of the air is in the troposphere but also highlights the relative importance of the prior profile shape in the troposphere, which could be particularly relevant where emissions take place. In addition, other metrics (such as the mean difference and standard deviation in the troposphere and stratosphere) were tested, and they resulted in similar conclusions.

5. Conclusions

High latitude methane emissions and their evolution in the warming Arctic are an intriguing and important subject of research, especially using novel Earth observations for added information. To support and enhance the use of TROPOMI satellite observations of methane in flux-inversion studies as well as to facilitate satellite-data-driven emission estimation, we have, in this work, carried out a systematic evaluation of the TROPOMI methane products and their recent version development, focusing exclusively on high latitudes (>50°N). The evaluation covers the years 2018–2021.

TROPOMI OPER rpro and WFMD v1.8 XCH_4 products were compared spatially, temporally, and latitudinally. The inter-product differences showed a systematically lower average XCH_4 for OPER rpro than for WFMD v1.8, except in the late winter and early spring months when OPER rpro exhibited higher values. In May, the difference (OPER rpro–WFMD v1.8) became systematically negative, persisting for most of the year. The spatial differences were the smallest in July. In the spatial scales of a few hundred kilometers, approximately ±30–40 ppb differences between the products could be found, especially over Canada as well as Russia. These spatial difference patterns were more profound in the first 5 months of each year, which might suggest snow-related interference. In the latter part of each year, the largest differences were found along the coasts of Greenland, suggesting a surface topography-related difference in the retrievals [29]. While an inter-product difference cannot be used for the validation of either product, the availability of several XCH_4 products based on different retrievals is important for a more reliable interpretation of spatial patterns and anomalous XCH_4 values as well as in supporting the evaluation of the overall reliability and robustness of the observations and retrieval approaches.

Comparisons against the ground-based reference measurements from four high-latitude TCCON and five COCCON stations were carried out in order to quantify the accuracy and precision of the TROPOMI products. The averages of the daily median XCH_4 differences are collected in Figure 20. The key findings are summarized as follows. TROPOMI products showed systematically mostly higher XCH_4 values compared to the TCCON, especially at the highest latitudes. The TROPOMI products were mostly in agreement with each other, except at St. Petersburg's campaign-related, shorter-term site. The similarity of the residual biases may refer to systematic errors in the products. The persistent seasonal bias in the OPER rpro data shown in this work and also pointed out by Lorente et al. [31] is reflected in the systematically larger scatter of OPER rpro compared to WFMD v1.8. Any residual and seasonal biases in the retrieval products can significantly affect the emission estimates from flux inversions and complicate their interpretation, especially when emissions with a strong seasonal variability, such as high-latitude wetland emissions, are considered [75].

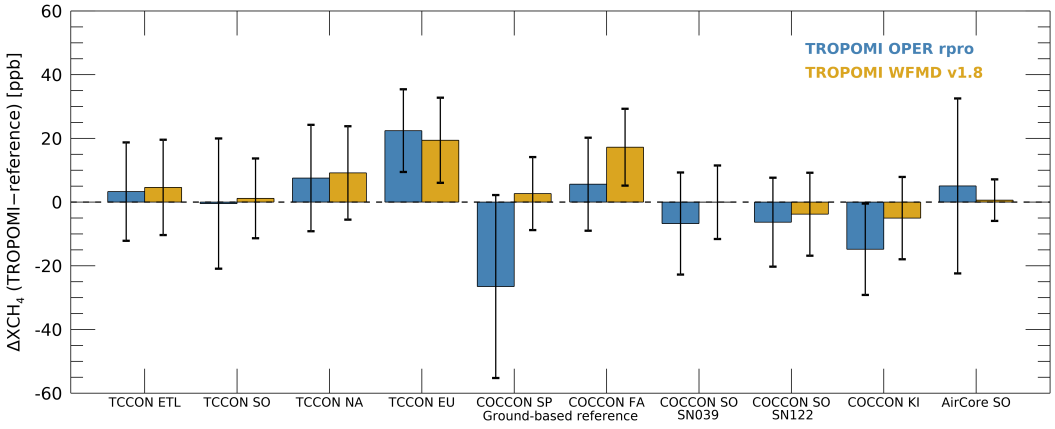

Figure 20. Collection of the TROPOMI high-latitude evaluation results obtained in this paper. The bar plots show the average difference of TROPOMI (OPER rpro or WFMD v1.8 product) and ground-based references, and the error bars depict the standard deviation. The references from left to right are TCCON stations at East Trout Lake, Sodankylä, Ny-Ålesund, and Eureka, then COCCON stations at St. Petersburg, Fairbanks, Sodankylä (SN039 and SN122), and Kiruna, and AirCore measurements at Sodankylä. It should be noted that the temporal sampling differs between the references.

A few remarks regarding high-latitude reference data are necessary. First, the accuracy and precision of satellite-retrieval products have improved significantly with matured algorithms, to the level where the accuracy and precision of the ground-based reference measurements have become essential. The recent updates in the TCCON GGG retrieval algorithm [45] had a decreasing impact of about 7 ppb (even larger at Eureka) to the

high-latitude TCCON data between versions GGG2014 and GGG2020. This is a significant fraction of the mean satellite-to-TCCON difference. While comparisons against the GGG2020 did not result systematically in improved TROPOMI-to-TCCON differences, the various updates made in the TCCON XCH_4 retrieval might give guidance to assess whether similar updates in prior profiles, spectroscopy, or other data processing would be necessary for the TROPOMI products, for collective improvements.

Second, localized site-to-site differences in the validation results also increase the importance of reliable reference data. In this study, the COCCON comparisons yielded systematic results that were quantitatively comparable to the TCCON, especially when the site latitude was taken into account. Shorter measurement periods (e.g., at St. Petersburg) can affect the representativeness and comparability of the result. Because the number of ground-based measurements at high latitudes remains severely limited, it is important to stress the value of the continuity, maintenance, characterization, and calibration of the measurements. As these reference measurements provide the primary validation data for multiple satellites, any temporal changes in their quality may indirectly affect the interpretation and even potential bias corrections of satellite data.

Measured atmospheric profiles of methane have proven useful in addition to the ground-based total column retrievals: they can be extrapolated to total atmospheric columns that provide another reference for the evaluation of TROPOMI XCH_4 products. The measured profiles can also give guidance to assessing the retrieval prior profile shapes for ground-based remote sensing as well as satellite observations. The analysis initiated in this study for evaluating the prior profile shape's significance at different altitudes for explaining the XCH_4 difference could be developed further, yet keeping in mind that the satellite XCH_4 retrievals are sensitive to a number of other factors as well. A key finding from the AirCore comparisons was that the tropospheric part of the prior profile shape was more important than the stratospheric part for explaining the differences in the total column, which is reasonable given that a majority of air (and methane) is in the troposphere. However, what about the variability within the troposphere—how significant is it to consider enhancements by local emissions in the boundary-layer part of the profile? The measured profiles can also be used for independent validation of ground-based retrievals and for linking to the WMO trace gas scales. This underlines the emerging need for more atmospheric profile measurements that would cover all seasons, either from balloon-borne AirCore or aircraft measurements. In addition, it would be important to further advance methane profile retrieval development for ground-based instruments into a more operational direction, perhaps using principal components and dimension reduction methods as presented by Karppinen et al. [27]. These would also serve as independent model evaluation data to the inverse modeling community.

To conclude, satellite observations of atmospheric methane from TROPOMI OPER rpro and WFMD v1.8 products enable seasonal analyses at high latitudes, even over permafrost regions. The data products have significantly improved over recent version updates, and the differences between the two products are mostly comparable in magnitude to their differences against the ground-based references. While some remaining spatial differences may complicate the interpretation of methane anomalies, especially in the winter and spring months, the agreement between the products in the summer and autumn suggests the possibility to make reliable satellite observations during the season of the highest natural methane emissions and the warming autumn, including the soil freezing period. Addressing the uncertainties related to the Arctic methane emissions and their evolution requires, in addition to reliable satellite observations, an improved understanding of complex carbon cycle and cryosphere interaction processes and their transfer to advanced models, as well as the disentanglement of anthropogenic and natural emissions.

Author Contributions: Conceptualization, H.L. and A.T.; methodology, H.L., E.K. and T.H.; software, H.L., E.K. and T.H.; formal analysis, H.L., E.K. and T.H.; data curation, O.S., M.B. (Michael Buchwitz), A.L., M.M.V., T.B., C.A., L.B., M.B. (Matthias Buschmann), H.C., D.D., F.H., P.H., T.K., R.K., E.M., J.N., S.R., W.S., K.S., Q.T. and D.W.; writing—original draft preparation, H.L., E.K., T.H., T.K., R.K., K.R. and D.W.; writing—review and editing, all authors; visualization, E.K., H.L. and T.H.; supervision, H.L. All authors have read and agreed to the published version of the manuscript.

Funding: This research was partially funded by the European Space Agency projects MethaneCamp and AMPAC-net. FMI team acknowledges funding from the Research Council of Finland grant numbers 337552, 331829, 351311, 359196, 353082, and 350184. E.K. acknowledges funding from the Tiina and Antti Herlin Foundation (Projects 20180222 and 20190003). R.K., P.H., and H.C. acknowledge funding provided by the ESA FRM4GHG project. The generation of the Bremen WFMD XCH_4 product has received co-funding from the ESA via project GHG-CCI. KIT is supported by ESA for developing COCCON in the framework of the COCCON-PROCEEDS I–III projects (grant no. 4000121212/17/I-EF), the COCCON-OPERA project (grant no. 4000140431/23/I-DT-Ir), and the FRM4GHG I + II projects (grant no. 4000117640/16/1-LG and no. 4000136108/21/I-DT-lr). The FRM4GHG support enabled the deployment of COCCON spectrometers in Sodankylä. The Eureka TCCON measurements were made at PEARL by the Canadian Network for the Detection of Atmospheric Change (CANDAC), primarily supported by the Natural Sciences and Engineering Research Council of Canada, Environment and Climate Change Canada, and the Canadian Space Agency. Measurements in St. Petersburg have been supported by the European Commission, H2020 observation-based system for monitoring and verification of greenhouse gases (VERIFY (grant no. 776810)) and the Russian Foundation for Basic Research (grant no. 18-05-00011). Ma.B. and J.N. thankfully acknowledge the funding by the Deutsche Forschungsgemeinschaft DFG (German Research Foundation)—project number 268020496—TRR 172, within the "Transregional Collaborative Research Center 'ArctiC Amplification: Climate Relevant Atmospheric and SurfaCe Processes, and Feedback Mechanisms (AC)3'".

Data Availability Statement: We acknowledge all colleagues providing the following data for high-latitude validation: TROPOMI XCH_4 products operational XCH_4 product [30], Bremen WFMD XCH_4 product [34,35], and SRON scientific product [31]. TCCON retrievals: Sodankylä (https://doi.org/10.14291/tccon.ggg2014.sodankyla01.R0/1149280), East Trout Lake (https://doi.org/10.14291/tccon.ggg2014.easttroutlake01.R0/1348207), Ny-Ålesund (https://doi.org/10.14291/TCCON.GGG2014.NYALESUND01.R1), and Eureka (http://doi.org/10.14291/tccon.ggg2014.eureka01.R2). COCCON: https://www.imk-asf.kit.edu/english/3884.php, accessed on 15 January 2023. Auxiliary data: ESA CCI-Permafrost Level 4.

Acknowledgments: We acknowledge the technical staff that contributed to the production of ground-based validation data. KIT acknowledges Uwe Raffalski, IRF Kiruna, for supporting the COCCON measurements conducted in Kiruna. KIT acknowledges Maria Makarova, Dmitry Ionov, Vladimir Kostsov, and Yana Virolainen from St Petersburg State University for their support of the St Petersburg COCCON campaign.

Conflicts of Interest: The authors declare no conflicts of interest. The funders had no role in the design of the study; in the collection, analyses, or interpretation of data; in the writing of the manuscript, or in the decision to publish the results.

Appendix A. TROPOMI OPER and WFMD v1.2 Time Series at the TCCON Sites

This Section includes the time series comparisons of TROPOMI daily median XCH_4 against the TCCON GGG2020 for the earlier TROPOMI product versions OPER and WFMD v1.2. These products have been used in the methane flux inversions in a paper prepared in parallel to the present one by Tsuruta et al. [75], which merits the evaluation of the products here, although newer product versions have already been introduced. Figures A1–A4 show the time series of the daily median XCH_4 for TROPOMI products and their comparison to the TCCON GGG2020, as well as their difference.

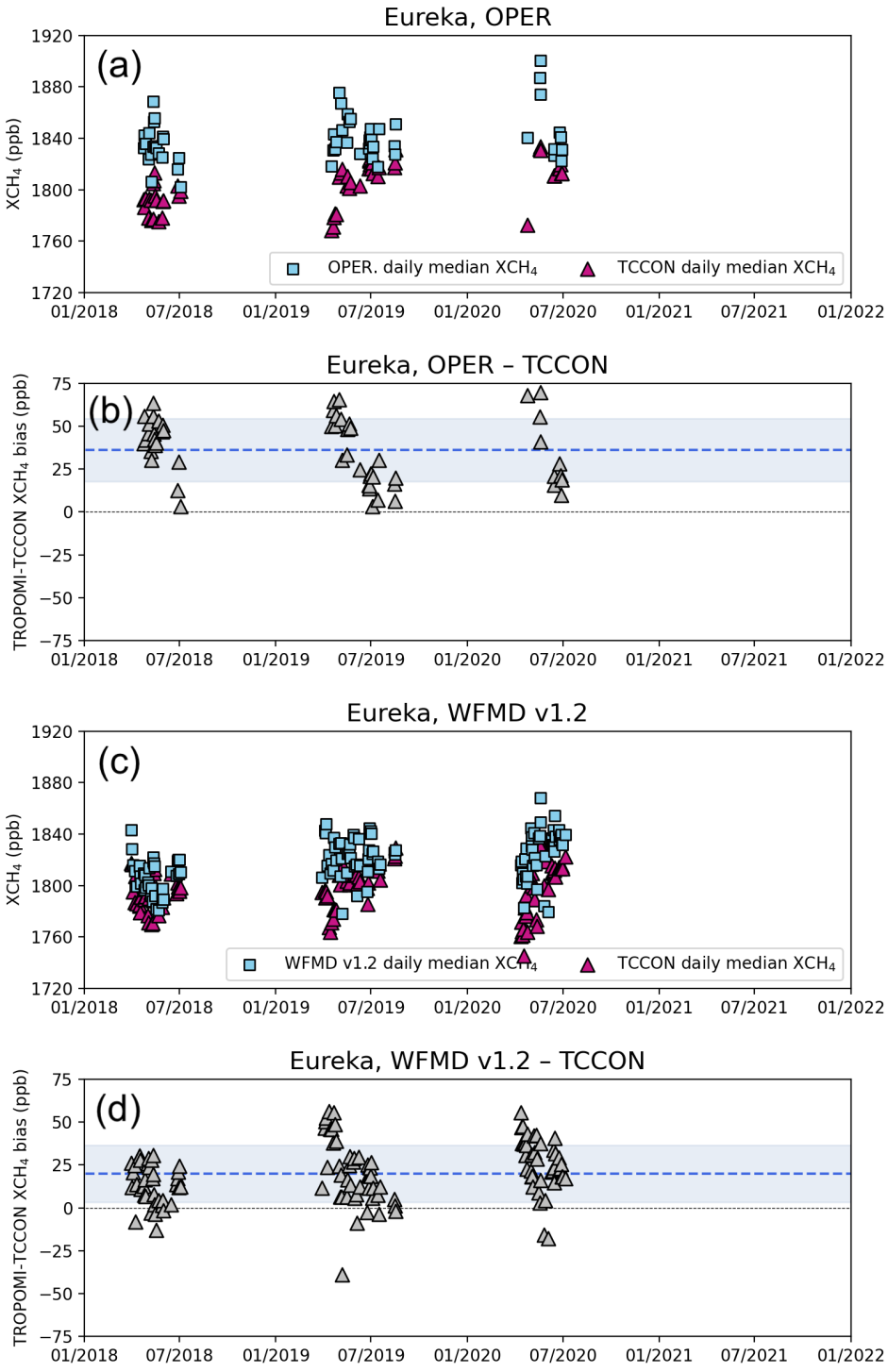

Figure A1. TCCON GGG2020 (blue) and co-located TROPOMI daily median XCH_4 (red) with (**a**) OPER and (**c**) WFMD v1.2 retrievals, and TROPOMI−TCCON differences (**b**,**d**) at Eureka (Canada) TCCON site. The dashed line in (**b**,**d**) show the mean difference at the site and shaded area the standard deviation of the mean.

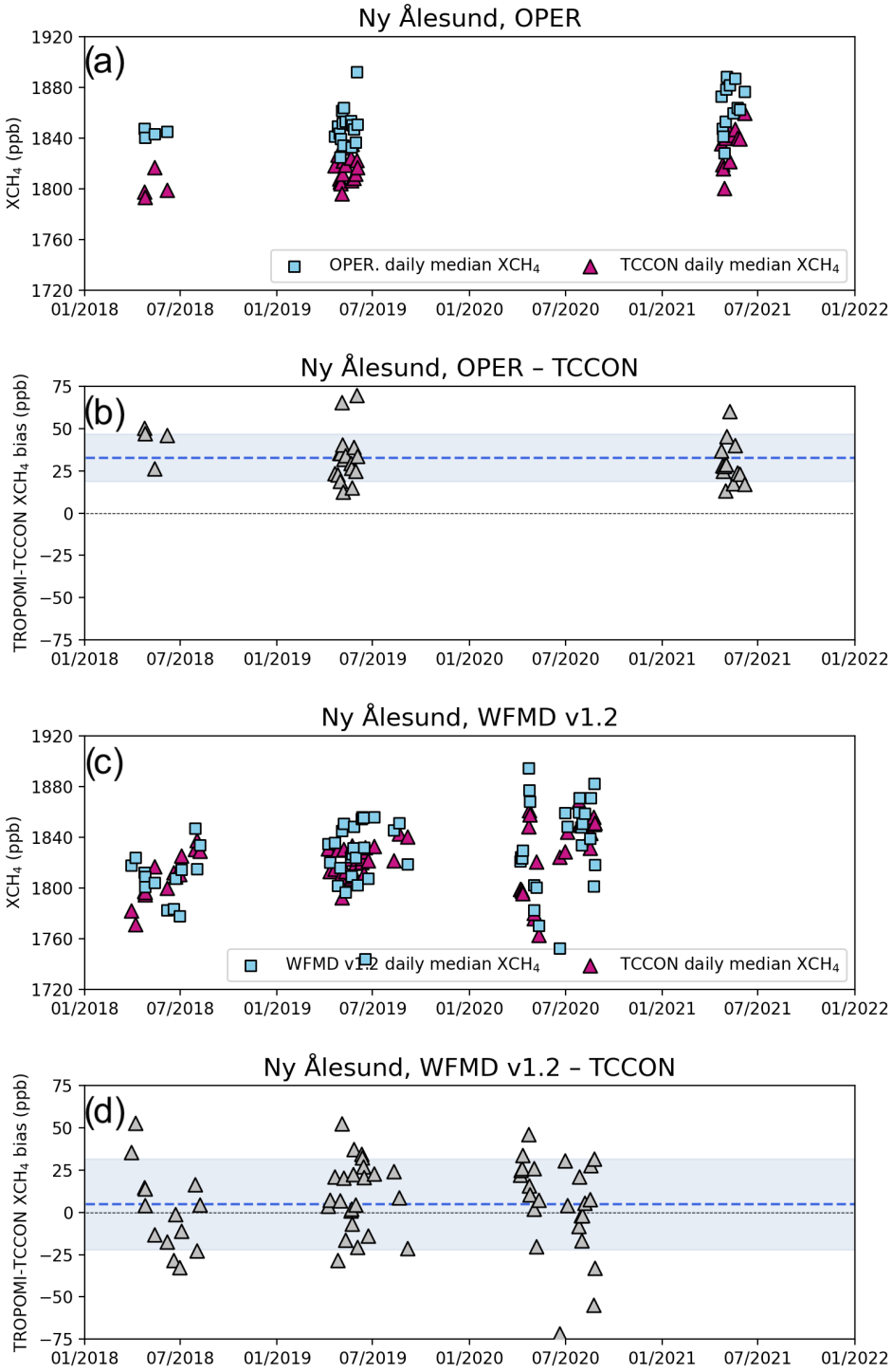

Figure A2. TCCON GGG2020 (blue) and co-located TROPOMI daily median XCH_4 (red) with (**a**) OPER and (**c**) WFMD v1.2 retrievals, and TROPOMI−TCCON differences (**b**,**d**) at Ny-Ålesund (Norway) TCCON site. The dashed line in (**b**,**d**) show the mean difference at the site and shaded area the standard deviation of the mean.

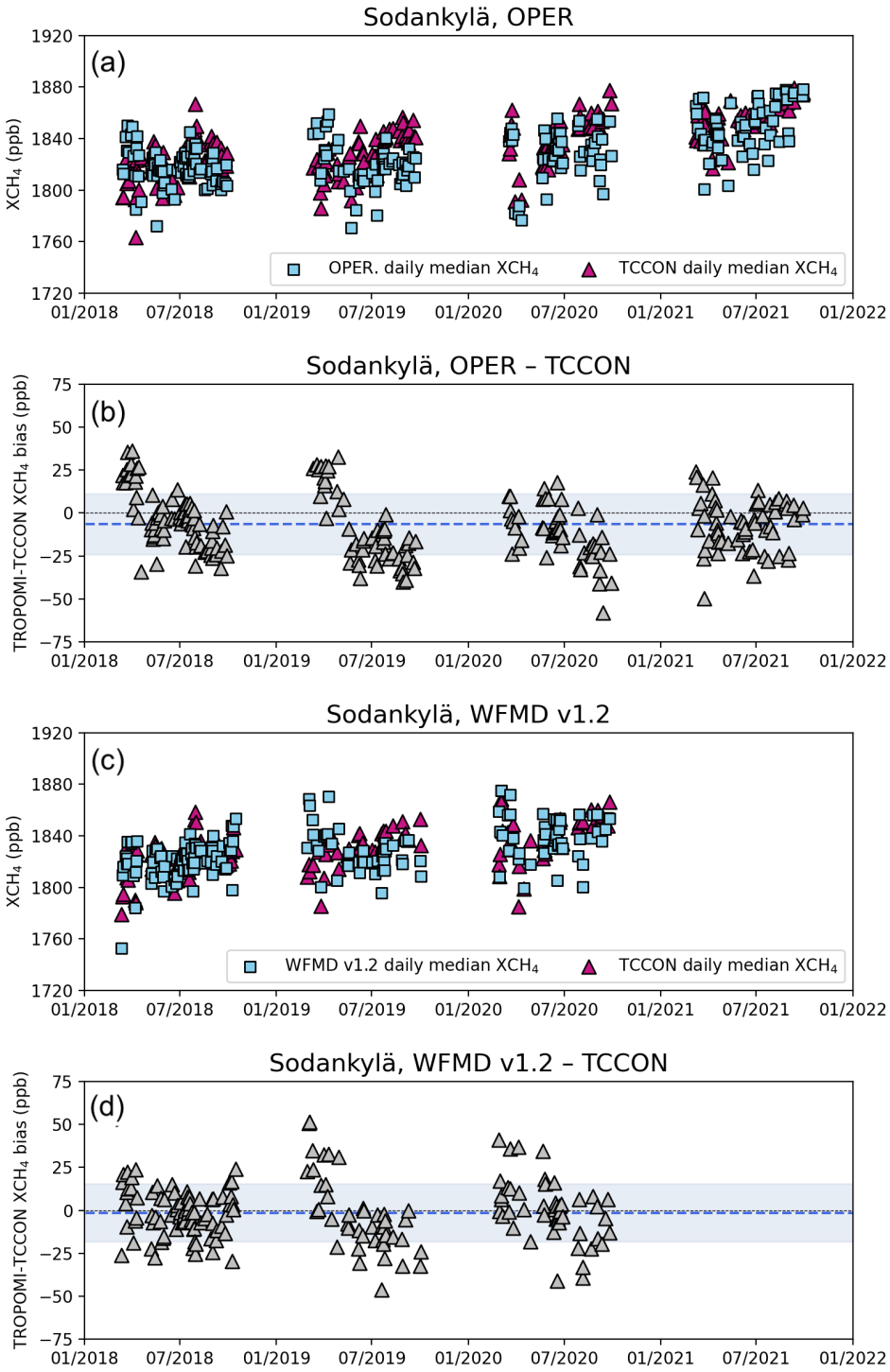

Figure A3. TCCON GGG2020 (blue) and co-located TROPOMI daily median XCH_4 (red) with (**a**) OPER and (**c**) WFMD v1.2 retrievals, and TROPOMI−TCCON differences (**b**,**d**) at Sodankylä (Finland) TCCON site. The dashed line in (**b**,**d**) show the mean difference at the site and shaded area the standard deviation of the mean.

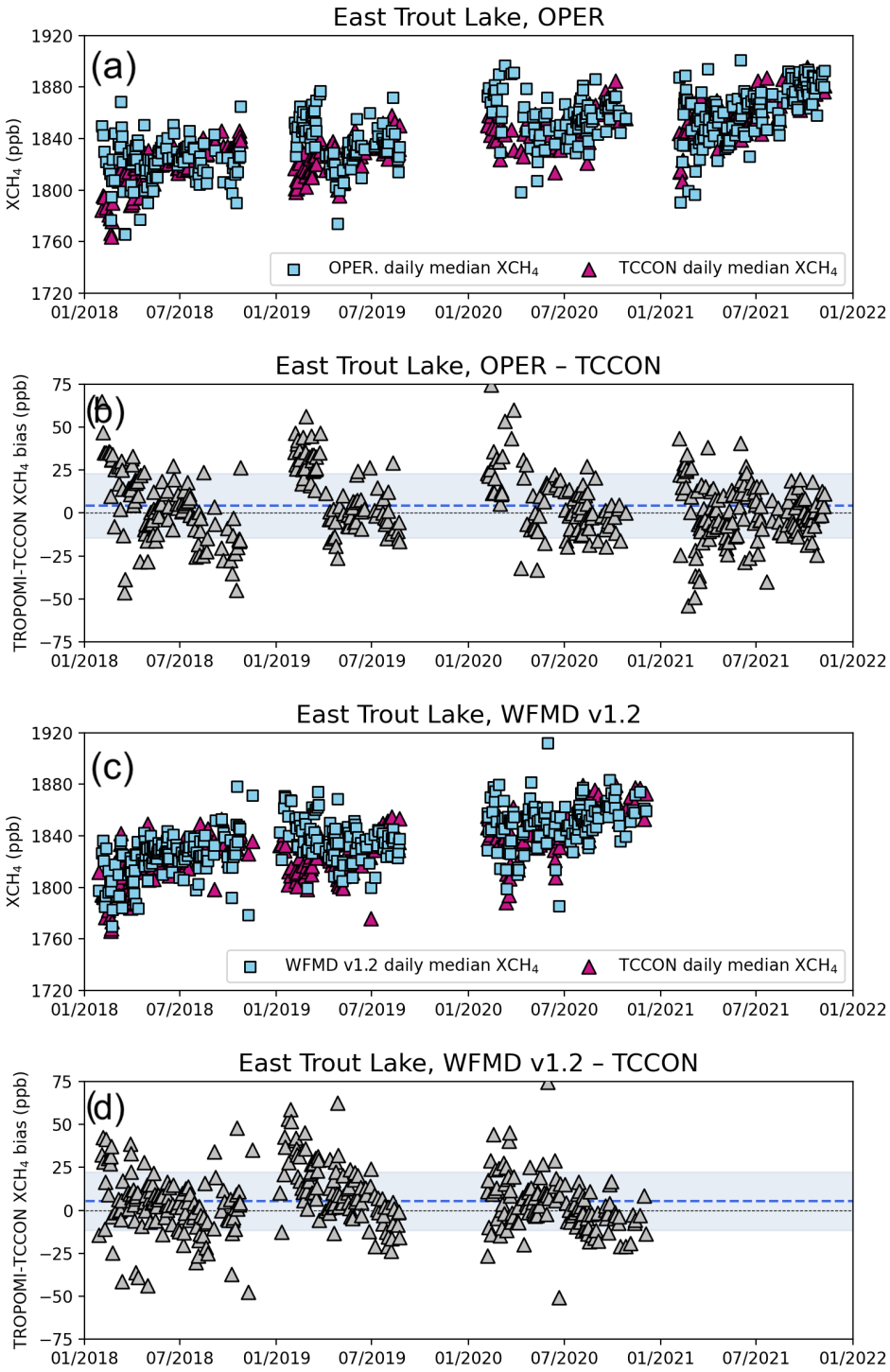

Figure A4. TCCON GGG2020 (blue) and co-located TROPOMI daily median XCH_4 (red) with (**a**) OPER and (**c**) WFMD v1.2 retrievals, and TROPOMI−TCCON differences (**b**,**d**) at East Trout Lake (Canada) TCCON site. The dashed line in (**b**,**d**) show the mean difference at the site and shaded area the standard deviation of the mean.

Appendix B. Tabulated Daily Median XCH_4 Differences

Table A1. TROPOMI–TCCON GGG2020 differences in the daily median XCH_4 values (calculated for 2018–2021, and including the following sampling differences: OPER rpro starts later than OPER, and WFMD v1.2 time series ends by the end of 2020).

	East Trout Lake	Sodankylä	Ny-Ålesund	Eureka
N, OPER rpro	462	270	48	79
Bias (ppb), OPER rpro	3.30	−0.47	7.54	22.42
1σ (ppb), OPER rpro	15.45	20.43	16.7	12.98
r, OPER rpro	0.604	0.415	0.494	0.761
N, WFMD v1.8	520	234	66	113
Bias (ppb), WFMD v1.8	4.61	1.17	9.17	19.41
1σ (ppb), WFMD v1.8	14.97	12.51	14.66	13.37
r , WFMD v1.8	0.744	0.707	0.847	0.643
N, OPER	444	259	34	56
Bias (ppb), OPER	4.22	−6.42	32.81	36.25
1σ (ppb), OPER	18.72	17.61	13.96	18.30
N, WFMD v1.2	377	172	64	126
Bias (ppb), WFMD v1.2	5.54	−1.43	4.79	19.98
1σ (ppb), WFMD v1.2	16.97	16.83	26.78	16.52

Table A2. TROPOMI–TCCON GGG2020 and TROPOMI–TCCON GGG2014 differences in the daily median XCH_4 values. The sampling and temporal co-location criteria are different compared to the data in Table A1. Here, all same-day observations were considered, and only the days with both GGG versions data are included.

	East Trout Lake	Sodankylä	Ny-Ålesund	Eureka
N, OPER rpro	363	295	44	77
Bias (ppb), GGG2014	−3.8	−12.9	−1.7	6.3
1σ (ppb), GGG2014	15.3	19.4	17.8	10.5
Bias (ppb), GGG2020	3.3	−6.3	5.6	21.9
1σ (ppb), GGG2020	16.6	19.9	18.3	10.3
N, WFMD v1.8	416	249	46	94
Bias (ppb), GGG2014	0.8	−4.3	− 0.9	9.0
1σ (ppb), GGG2014	14.2	12.3	18.0	13.1
Bias (ppb), GGG2020	8.9	3.3	10.5	25.3
1σ (ppb), GGG2020	15.3	13.0	20.1	14.1

Table A3. TROPOMI–COCCON differences in the daily median XCH_4 values and correlations *r* for OPER rpro and WFMD v1.8.

	Kiruna	Sodankylä (SN039)	Sodankylä (SN122)	Fairbanks	St. Petersburg
N, OPER rpro	125	97	40	205	15
Bias (ppb), OPER rpro	−14.81	−6.74	−6.32	5.62	−26.51
1σ (ppb), OPER rpro	14.36	16.02	13.96	14.61	28.73
r, OPER rpro	0.561	0.368	0.750	0.712	0.118
N, WFMD v1.8	132	78	27	188	27
Bias (ppb), WFMD v1.8	−5.03	−0.03	−3.79	17.23	2.67
1σ (ppb), WFMD v1.8	12.94	11.54	13.02	12.05	11.45
r, WFMD v1.8	0.734	0.576	0.595	0.819	0.623

References

1. Rantanen, M.; Karpechko, A.Y.; Lipponen, A.; Nordling, K.; Hyvärinen, O.; Ruosteenoja, K.; Vihma, T.; Laaksonen, A. The Arctic has warmed nearly four times faster than the globe since 1979. *Commun. Earth Environ.* **2022**, *3*, 168. [CrossRef]
2. Comiso, J.C.; Hall, D.K. Climate trends in the Arctic as observed from space. *Wiley Interdiscip. Rev. Clim. Chang.* **2014**, *5*, 389–409. [CrossRef] [PubMed]
3. Pulliainen, J.; Luojus, K.; Derksen, C.; Mudryk, L.; Lemmetyinen, J.; Salminen, M.; Ikonen, J.; Takala, M.; Cohen, J.; Smolander, T.; et al. Patterns and trends of Northern Hemisphere snow mass from 1980 to 2018. *Nature* **2020**, *581*, 294–298. [CrossRef] [PubMed]
4. Runge, A.; Nitze, I.; Grosse, G. Remote sensing annual dynamics of rapid permafrost thaw disturbances with LandTrendr. *Remote Sens. Environ.* **2022**, *268*, 112752. [CrossRef]
5. Shiklomanov, N.I.; Streletskiy, D.A.; Nelson, F.E. Northern hemisphere component of the global circumpolar active layer monitoring (CALM) program. In Proceedings of the 10th International Conference on Permafrost, Salekhard, Russia, 25–29 June 2012; Volume 1, pp. 377–382.
6. Henry, H.A. Climate change and soil freezing dynamics: Historical trends and projected changes. *Clim. Chang.* **2008**, *87*, 421–434. [CrossRef]
7. Paxian, A.; Eyring, V.; Beer, W.; Sausen, R.; Wright, C. Present-day and future global bottom-up ship emission inventories including polar routes. *Environ. Sci. Technol.* **2010**, *44*, 1333–1339. [CrossRef] [PubMed]
8. Schach, M.; Madlener, R. Impacts of an ice-free Northeast Passage on LNG markets and geopolitics. *Energy Policy* **2018**, *122*, 438–448. [CrossRef]
9. Petrick, S.; Riemann-Campe, K.; Hoog, S.; Growitsch, C.; Schwind, H.; Gerdes, R.; Rehdanz, K. Climate change, future Arctic Sea ice, and the competitiveness of European Arctic offshore oil and gas production on world markets. *Ambio* **2017**, *46*, 410–422. [CrossRef]
10. Turetsky, M.R.; Abbott, B.W.; Jones, M.C.; Anthony, K.W.; Olefeldt, D.; Schuur, E.A.; Grosse, G.; Kuhry, P.; Hugelius, G.; Koven, C.; et al. Carbon release through abrupt permafrost thaw. *Nat. Geosci.* **2020**, *13*, 138–143. [CrossRef]
11. Miner, K.R.; Turetsky, M.R.; Malina, E.; Bartsch, A.; Tamminen, J.; McGuire, A.D.; Fix, A.; Sweeney, C.; Elder, C.D.; Miller, C.E. Permafrost carbon emissions in a changing Arctic. *Nat. Rev. Earth Environ.* **2022**, *3*, 55–67. [CrossRef]
12. Comiso, J.C.; Parkinson, C.L. Satellite-observed changes in the Arctic. *Phys. Today* **2004**, *57*, 38–44. [CrossRef]
13. Duncan, B.N.; Ott, L.E.; Abshire, J.B.; Brucker, L.; Carroll, M.L.; Carton, J.; Comiso, J.C.; Dinnat, E.P.; Forbes, B.C.; Gonsamo, A.; et al. Space-based observations for understanding changes in the arctic-boreal zone. *Rev. Geophys.* **2020**, *58*, e2019RG000652. [CrossRef]
14. Buchwitz, M.d.; De Beek, R.; Burrows, J.; Bovensmann, H.; Warneke, T.; Notholt, J.; Meirink, J.; Goede, A.; Bergamaschi, P.; Körner, S.; et al. Atmospheric methane and carbon dioxide from SCIAMACHY satellite data: Initial comparison with chemistry and transport models. *Atmos. Chem. Phys.* **2005**, *5*, 941–962. [CrossRef]
15. Kuze, A.; Suto, H.; Nakajima, M.; Hamazaki, T. Thermal and near infrared sensor for carbon observation Fourier-transform spectrometer on the Greenhouse Gases Observing Satellite for greenhouse gases monitoring. *Appl. Opt.* **2009**, *48*, 6716–6733. [CrossRef] [PubMed]
16. Tsuruta, A.; Aalto, T.; Backman, L.; Hakkarainen, J.; Van Der Laan-Luijkx, I.T.; Krol, M.C.; Spahni, R.; Houweling, S.; Laine, M.; Dlugokencky, E.; et al. Global methane emission estimates for 2000–2012 from CarbonTracker Europe-CH 4 v1. 0. *Geosci. Model Dev.* **2017**, *10*, 1261–1289. [CrossRef]
17. Maasakkers, J.D.; Jacob, D.J.; Sulprizio, M.P.; Scarpelli, T.R.; Nesser, H.; Sheng, J.X.; Zhang, Y.; Hersher, M.; Bloom, A.A.; Bowman, K.W.; et al. Global distribution of methane emissions, emission trends, and OH concentrations and trends inferred from an inversion of GOSAT satellite data for 2010–2015. *Atmos. Chem. Phys.* **2019**, *19*, 7859–7881. [CrossRef]
18. Baray, S.; Jacob, D.J.; Maasakkers, J.D.; Sheng, J.X.; Sulprizio, M.P.; Jones, D.B.; Bloom, A.A.; McLaren, R. Estimating 2010–2015 anthropogenic and natural methane emissions in Canada using ECCC surface and GOSAT satellite observations. *Atmos. Chem. Phys.* **2021**, *21*, 18101–18121. [CrossRef]
19. Veefkind, J.P.; Aben, I.; McMullan, K.; Förster, H.; De Vries, J.; Otter, G.; Claas, J.; Eskes, H.; De Haan, J.; Kleipool, Q.; et al. TROPOMI on the ESA Sentinel-5 Precursor: A GMES mission for global observations of the atmospheric composition for climate, air quality and ozone layer applications. *Remote Sens. Environ.* **2012**, *120*, 70–83. [CrossRef]
20. Liu, M.; Van Der A, R.; Van Weele, M.; Eskes, H.; Lu, X.; Veefkind, P.; De Laat, J.; Kong, H.; Wang, J.; Sun, J.; et al. A new divergence method to quantify methane emissions using observations of Sentinel-5P TROPOMI. *Geophys. Res. Lett.* **2021**, *48*, e2021GL094151. [CrossRef]
21. Jacob, D.J.; Varon, D.J.; Cusworth, D.H.; Dennison, P.E.; Frankenberg, C.; Gautam, R.; Guanter, L.; Kelley, J.; McKeever, J.; Ott, L.E.; et al. Quantifying methane emissions from the global scale down to point sources using satellite observations of atmospheric methane. *Atmos. Chem. Phys.* **2022**, *22*, 9617–9646. [CrossRef]
22. Schneising, O.; Buchwitz, M.; Reuter, M.; Vanselow, S.; Bovensmann, H.; Burrows, J.P. Remote sensing of methane leakage from natural gas and petroleum systems revisited. *Atmos. Chem. Phys.* **2020**, *20*, 9169–9182. [CrossRef]
23. Ialongo, I.; Stepanova, N.; Hakkarainen, J.; Virta, H.; Gritsenko, D. Satellite-based estimates of nitrogen oxide and methane emissions from gas flaring and oil production activities in Sakha Republic, Russia. *Atmos. Environ. X* **2021**, *11*, 100114. [CrossRef]

24. Lindqvist, H.; Martikainen, J.; Räbinä, J.; Penttilä, A.; Muinonen, K. Ray optics for absorbing particles with application to ice crystals at near-infrared wavelengths. *J. Quant. Spectrosc. Radiat. Transf.* **2018**, *217*, 329–337. [CrossRef]
25. Mikkonen, A.; Lindqvist, H.; Peltoniemi, J.; Tamminen, J. Non-Lambertian snow surface reflection models for simulated top-of-the-atmosphere radiances in the NIR and SWIR wavelengths. *J. Quant. Spectrosc. Radiat. Transf.* **2024**, *315*, 108892. [CrossRef]
26. Tukiainen, S.; Railo, J.; Laine, M.; Hakkarainen, J.; Kivi, R.; Heikkinen, P.; Chen, H.; Tamminen, J. Retrieval of atmospheric CH4 profiles from Fourier transform infrared data using dimension reduction and MCMC. *J. Geophys. Res. Atmos.* **2016**, *121*, 10–312. [CrossRef]
27. Karppinen, T.; Lamminpää, O.; Tukiainen, S.; Kivi, R.; Heikkinen, P.; Hatakka, J.; Laine, M.; Chen, H.; Lindqvist, H.; Tamminen, J. Vertical distribution of arctic methane in 2009–2018 using ground-based remote sensing. *Remote Sens.* **2020**, *12*, 917. [CrossRef]
28. Boesch, H.; Liu, Y.; Tamminen, J.; Yang, D.; Palmer, P.I.; Lindqvist, H.; Cai, Z.; Che, K.; Di Noia, A.; Feng, L.; et al. Monitoring greenhouse gases from space. *Remote Sens.* **2021**, *13*, 2700. [CrossRef]
29. Hachmeister, J.; Schneising, O.; Buchwitz, M.; Lorente, A.; Borsdorff, T.; Burrows, J.P.; Notholt, J.; Buschmann, M. On the influence of underlying elevation data on Sentinel-5 Precursor TROPOMI satellite methane retrievals over Greenland. *Atmos. Meas. Tech.* **2022**, *15*, 4063–4074. [CrossRef]
30. Hu, H.; Landgraf, J.; Detmers, R.; Borsdorff, T.; Aan de Brugh, J.; Aben, I.; Butz, A.; Hasekamp, O. Toward global mapping of methane with TROPOMI: First results and intersatellite comparison to GOSAT. *Geophys. Res. Lett.* **2018**, *45*, 3682–3689. [CrossRef]
31. Lorente, A.; Borsdorff, T.; Butz, A.; Hasekamp, O.; aan de Brugh, J.; Schneider, A.; Wu, L.; Hase, F.; Kivi, R.; Wunch, D.; et al. Methane retrieved from TROPOMI: Improvement of the data product and validation of the first 2 years of measurements. *Atmos. Meas. Tech.* **2021**, *14*, 665–684. [CrossRef]
32. Lorente, A.; Borsdorff, T.; Martinez-Velarte, M.C.; Butz, A.; Hasekamp, O.P.; Wu, L.; Landgraf, J. Evaluation of the methane full-physics retrieval applied to TROPOMI ocean sun glint measurements. *Atmos. Meas. Tech.* **2022**, *15*, 6585–6603. [CrossRef]
33. Borsdorff, T.; Martinez-Velarte, M.C.; Sneep, M.; ter Linden, M.; Landgraf, J. Random Forest Classifier for Cloud Clearing of the Operational TROPOMI XCH4 Product. *Remote Sens.* **2024**, *16*, 1208. [CrossRef]
34. Schneising, O.; Buchwitz, M.; Reuter, M.; Bovensmann, H.; Burrows, J.P.; Borsdorff, T.; Deutscher, N.M.; Feist, D.G.; Griffith, D.W.T.; Hase, F.; et al. A scientific algorithm to simultaneously retrieve carbon monoxide and methane from TROPOMI onboard Sentinel-5 Precursor. *Atmos. Meas. Tech.* **2019**, *12*, 6771–6802. [CrossRef]
35. Schneising, O.; Buchwitz, M.; Hachmeister, J.; Vanselow, S.; Reuter, M.; Buschmann, M.; Bovensmann, H.; Burrows, J.P. Advances in retrieving XCH_4 and XCO from Sentinel-5 Precursor: Improvements in the scientific TROPOMI/WFMD algorithm. *Atmos. Meas. Tech.* **2023**, *16*, 669–694. [CrossRef]
36. Wu, L.; Hasekamp, O.; Hu, H.; Landgraf, J.; Butz, A.; Aben, I.; Pollard, D.F.; Griffith, D.W.; Feist, D.G.; Koshelev, D.; et al. Carbon dioxide retrieval from OCO-2 satellite observations using the RemoTeC algorithm and validation with TCCON measurements. *Atmos. Meas. Tech.* **2018**, *11*, 3111–3130. [CrossRef]
37. Butz, A.; Galli, A.; Hasekamp, O.; Landgraf, J.; Tol, P.; Aben, I. TROPOMI aboard Sentinel-5 Precursor: Prospective performance of CH4 retrievals for aerosol and cirrus loaded atmospheres. *Remote Sens. Environ.* **2012**, *120*, 267–276. [CrossRef]
38. Schepers, D.; Aan de Brugh, J.; Hahne, P.; Butz, A.; Hasekamp, O.; Landgraf, J. LINTRAN v2.0: A linearised vector radiative transfer model for efficient simulation of satellite-born nadir-viewing reflection measurements of cloudy atmospheres. *J. Quant. Spectrosc. Radiat. Transf.* **2014**, *149*, 347–359. [CrossRef]
39. Landgraf, J.; Hasekamp, O.P.; Box, M.A.; Trautmann, T. A linearized radiative transfer model for ozone profile retrieval using the analytical forward-adjoint perturbation theory approach. *J. Geophys. Res. Atmos.* **2001**, *106*, 27291–27305. [CrossRef]
40. Houweling, S.; Krol, M.; Bergamaschi, P.; Frankenberg, C.; Dlugokencky, E.; Morino, I.; Notholt, J.; Sherlock, V.; Wunch, D.; Beck, V.; et al. A multi-year methane inversion using SCIAMACHY, accounting for systematic errors using TCCON measurements. *Atmos. Chem. Phys.* **2014**, *14*, 3991–4012. [CrossRef]
41. Hasekamp, O.; Lorente, A.; Hu, H.; Butz, A.; de Brugh, J.; Landgraf, J. Algorithm Theoretical Baseline Document for Sentinel-5 Precursor Methane Retrieval. 2022. Available online: https://sentinels.copernicus.eu/documents/247904/2476257/Sentinel-5P-TROPOMI-ATBD-Methane-retrieval.pdf/f275eb1d-89a8-464f-b5b8-c7156cda874e?t=1658313508597 (accessed on 15 April 2024).
42. Lorente, A.; Borsdorff, T.; Martinez-Velarte, M.C.; Landgraf, J. Accounting for surface reflectance spectral features in TROPOMI methane retrievals. *Atmos. Meas. Tech.* **2023**, *16*, 1597–1608. [CrossRef]
43. Wunch, D.; Toon, G.C.; Wennberg, P.O.; Wofsy, S.C.; Stephens, B.B.; Fischer, M.L.; Uchino, O.; Abshire, J.B.; Bernath, P.; Biraud, S.C.; et al. Calibration of the Total Carbon Column Observing Network using aircraft profile data. *Atmos. Meas. Tech.* **2010**, *3*, 1351–1362. [CrossRef]
44. Wunch, D.; Toon, G.C.; Blavier, J.F.L.; Washenfelder, R.A.; Notholt, J.; Connor, B.J.; Griffith, D.W.T.; Sherlock, V.; Wennberg, P.O. The Total Carbon Column Observing Network. *Philos. Trans. R. Soc. A Math. Phys. Eng. Sci.* **2011**, *369*, 2087–2112. [CrossRef] [PubMed]
45. Laughner, J.L.; Toon, G.C.; Mendonca, J.; Petri, C.; Roche, S.; Wunch, D.; Blavier, J.F.; Griffith, D.W.; Heikkinen, P.; Keeling, R.F.; et al. The Total Carbon Column Observing Network's GGG2020 Data Version. *Earth Syst. Sci. Data Discuss.* **2023**, *2023*, 1–86. [CrossRef]

46. Laughner, J.L.; Roche, S.; Kiel, M.; Toon, G.C.; Wunch, D.; Baier, B.C.; Biraud, S.; Chen, H.; Kivi, R.; Laemmel, T.; et al. A new algorithm to generate a priori trace gas profiles for the GGG2020 retrieval algorithm. *Atmos. Meas. Tech.* **2023**, *16*, 1121–1146. [CrossRef]
47. Wunch, D.; Mendonca, J.; Colebatch, O.; Allen, N.; Blavier, J.F.L.; Springett, S.; Worthy, D.; Kessler, R.; Strong, K. *TCCON Data from East Trout Lake, Canada, Release GGG2014R0*; TCCON Data Archive; CaltechDATA, California Institute of Technology: Pasadena, CA, USA, 2014. [CrossRef]
48. Wunch, D.; Mendonca, J.; Colebatch, O.; Allen, N.; Blavier, J.F.L.; Kunz, K.; Roche, S.; Hedelius, J.; Neufeld, G.; Springett, S.; et al. *TCCON Data from East Trout Lake, Canada, Release GGG2020R0*; TCCON Data Archive; CaltechDATA, California Institute of Technology: Pasadena, CA, USA, 2020. [CrossRef]
49. Kivi, R.; Heikkinen, P. Fourier transform spectrometer measurements of column CO_2 at Sodankylä, Finland. *Geosci. Instrum. Method. Data Syst.* **2016**, *5*, 271–279. [CrossRef]
50. Kivi, R.; Heikkinen, P.; Kyrö, E. *TCCON Data from Sodankylä (FI), Release GGG2014.R0*; CaltechDATA, California Institute of Technology: Pasadena, CA, USA, 2014. [CrossRef]
51. Kivi, R.; Heikkinen, P.; Kyro, E. *TCCON Data from Sodankyla, Finland, Release GGG2020R0*; TCCON Data Archive; CaltechDATA, California Institute of Technology: Pasadena, CA, USA, 2017. [CrossRef]
52. Maturilli, M. *Basic and Other Measurements of Radiation at Station Ny-Ålesund (2006-05 et seq)*; Alfred Wegener Institute—Research Unit Potsdam, PANGAEA: Bremerhaven, Germany, 2020. [CrossRef]
53. Notholt, J.; Warneke, T.; Petri, C.; Deutscher, N.M.; Weinzierl, C.; Palm, M.; Buschmann, M. *TCCON Data from Ny Ålesund, Spitsbergen (NO), Release GGG2014.R1*; CaltechDATA: Pasadena, CA, USA, 2019. [CrossRef]
54. Buschmann, M.; Petri, C.; Palm, M.; Warneke, T.; Notholt, J.; Engineers, A.S. *TCCON Data from Ny-Alesund, Svalbard, Norway, Release GGG2020R0*; TCCON Data Archive; CaltechDATA, California Institute of Technology: Pasadena, CA, USA, 2022. [CrossRef]
55. Fogal, P.F.; LeBlanc, L.M.; Drummond, J.R. The polar environment atmospheric research laboratory (PEARL): Sounding the atmosphere at 80° North. *Arctic* **2013**, *66*, 377–386. [CrossRef]
56. Batchelor, R.L.; Strong, K.; Lindenmaier, R.; Mittermeier, R.L.; Fast, H.; Drummond, J.R.; Fogal, P.F. A new Bruker IFS 125HR FTIR spectrometer for the Polar Environment Atmospheric Research Laboratory at Eureka, Nunavut, Canada: Measurements and comparison with the existing Bomem DA8 spectrometer. *J. Atmos. Ocean. Technol.* **2009**, *26*, 1328–1340. [CrossRef]
57. Strong, K.; Roche, S.; Franklin, J.; Mendonca, J.; Lutsch, E.; Weaver, D.; Fogal, P.; Drummond, J.; Batchelor, R.; Lindenmaier, R. *TCCON Data from Eureka (CA), Release GGG2014. R3*; TCCON Data Archive; CaltechDATA: Pasadena, CA, USA, 2019.
58. Strong, K.; Roche, S.; Franklin, J.; Mendonca, J.; Lutsch, E.; Weaver, D.; Fogal, P.; Drummond, J.; Batchelor, R.; Lindenmaier, R.; et al. *TCCON Data from Eureka (CA), Release GGG2020. R0 (Version R0) [Data Set]*; CaltechDATA: Pasadena, CA, USA, 2022.
59. Frey, M.; Sha, M.K.; Hase, F.; Kiel, M.; Blumenstock, T.; Harig, R.; Surawicz, G.; Deutscher, N.M.; Shiomi, K.; Franklin, J.E.; et al. Building the COllaborative Carbon Column Observing Network (COCCON): Long-term stability and ensemble performance of the EM27/SUN Fourier transform spectrometer. *Atmos. Meas. Tech.* **2019**, *12*, 1513–1530. [CrossRef]
60. Gisi, M.; Hase, F.; Dohe, S.; Blumenstock, T.; Simon, A.; Keens, A. XCO_2-measurements with a tabletop FTS using solar absorption spectroscopy. *Atmos. Meas. Tech.* **2012**, *5*, 2969–2980. [CrossRef]
61. Hase, F.; Frey, M.; Kiel, M.; Blumenstock, T.; Harig, R.; Keens, A.; Orphal, J. Addition of a channel for XCO observations to a portable FTIR spectrometer for greenhouse gas measurements. *Atmos. Meas. Tech.* **2016**, *9*, 2303–2313. [CrossRef]
62. Sha, M.K.; De Mazière, M.; Notholt, J.; Blumenstock, T.; Chen, H.; Dehn, A.; Griffith, D.W.T.; Hase, F.; Heikkinen, P.; Hermans, C.; et al. Intercomparison of low- and high-resolution infrared spectrometers for ground-based solar remote sensing measurements of total column concentrations of CO_2, CH_4, and CO. *Atmos. Meas. Tech.* **2020**, *13*, 4791–4839. [CrossRef]
63. Alberti, C.; Hase, F.; Frey, M.; Dubravica, D.; Blumenstock, T.; Dehn, A.; Castracane, P.; Surawicz, G.; Harig, R.; Baier, B.C.; et al. Improved calibration procedures for the EM27/SUN spectrometers of the COllaborative Carbon Column Observing Network (COCCON). *Atmos. Meas. Tech.* **2022**, *15*, 2433–2463. [CrossRef]
64. Blumenstock, T.; Roehling, A.; Raffalski, U.; Dubravica, D. *COCCON Version 1 Dataset from Atmospheric Observatory of Kiruna Available at the EVDC Data Handling Facilities Covering Start Date Mar 9th 2017 to End Date Apr 21th 2020*; COCCON—Central Facility/EVDC—ESA Atmospheric Validation Data Centre: Paris, France, 2021. [CrossRef]
65. Tu, Q.; Hase, F.; Blumenstock, T.; Kivi, R.; Heikkinen, P.; Sha, M.K.; Raffalski, U.; Landgraf, J.; Lorente, A.; Borsdorff, T.; et al. Intercomparison of atmospheric CO_2 and CH_4 abundances on regional scales in boreal areas using Copernicus Atmosphere Monitoring Service (CAMS) analysis, COllaborative Carbon Column Observing Network (COCCON) spectrometers, and Sentinel-5 Precursor satellite observations. *Atmos. Meas. Tech.* **2020**, *13*, 4751–4771. [CrossRef]
66. Tu, Q.; Heikkinen, P.; Dubravica, D. *COCCON Version 1 Dataset from Atmospheric Observatory of Sodankyla Available at the EVDC Data Handling Facilities Covering Start Date Mar 6th 2017 to End Date Jun 2nd 2020*; COCCON—Central Facility/EVDC—ESA Atmospheric Validation Data Centre: Paris, France, 2021. [CrossRef]
67. Kivi, R.; Heikkinen, P. *COCCON Version 1 Dataset from Atmospheric Observatory of Sodankyla Available at the EVDC Data Handling Facilities Covering Start Date Apr 2nd 2020 to End Date Mar 23rd 2021*; COCCON—Central Facility/EVDC—ESA Atmospheric Validation Data Centre: Paris, France, 2023. [CrossRef]

68. Simpson, W.; Jacobs, N. *COCCON Version 1 Dataset from Atmospheric Observatory of Fairbanks/Alaska Available at the EVDC Data Handling Facilities Covering Start Date Apr 7th 2018 to End Date Oct 18th 2021*; COCCON—Central Facility/EVDC—ESA Atmospheric Validation Data Centre: Paris, France, 2022. [CrossRef]
69. Hase, F.; Alberti, C.; Dubravica, D.; Makarova, M.; Foka, S. *COCCON Version 1 Dataset from Atmospheric Observatory of Saint Petersburg Available at the EVDC Data Handling Facilities Covering Start Date Jan 22nd 2019 to End date Mar 17th 2020*; COCCON—Central Facility/EVDC—ESA Atmospheric Validation Data Centre: Paris, France, 2022. [CrossRef]
70. Alberti, C.; Tu, Q.; Hase, F.; Makarova, M.V.; Gribanov, K.; Foka, S.C.; Zakharov, V.; Blumenstock, T.; Buchwitz, M.; Diekmann, C.; et al. Investigation of spaceborne trace gas products over St Petersburg and Yekaterinburg, Russia, by using COllaborative Column Carbon Observing Network (COCCON) observations. *Atmos. Meas. Tech.* **2022**, *15*, 2199–2229. [CrossRef]
71. Karion, A.; Sweeney, C.; Tans, P.; Newberger, T. AirCore: An Innovative Atmospheric Sampling System. *J. Atmos. Ocean. Technol.* **2010**, *27*, 1839–1853. [CrossRef]
72. Osterkamp, T.; Burn, C. PERMAFROST. In *Encyclopedia of Atmospheric Sciences*; Holton, J.R., Ed.; Academic Press: Oxford, UK, 2003; pp. 1717–1729. [CrossRef]
73. Obu, J.; Westermann, S.; Barboux, C.; Bartsch, A.; Delaloye, R.; Grosse, G.; Heim, B.; Hugelius, G.; Irrgang, A.; Kääb, A.; et al. *ESA Permafrost Climate Change Initiative (Permafrost_cci): Permafrost Version 3 Data Products*; Centre for Environmental Data Analysis: Oxfordshire, UK, 2024.
74. Rodgers, C.D. *Inverse Methods for Atmospheric Sounding: Theory and Practice*; World Scientific: Singapore, 2000; Volume 2.
75. Tsuruta, A.; Kivimäki, E.; Lindqvist, H.; Karppinen, T.; Backman, L.; Hakkarainen, J.; Schneising, O.; Buchwitz, M.; Lan, X.; Kivi, R.; et al. CH4 Fluxes Derived from Assimilation of TROPOMI XCH4 in CarbonTracker Europe-CH4: Evaluation of Seasonality and Spatial Distribution in the Northern High Latitudes. *Remote Sens.* **2023**, *15*, 1620. [CrossRef]
76. Mostafavi Pak, N.; Hedelius, J.K.; Roche, S.; Cunningham, L.; Baier, B.; Sweeney, C.; Roehl, C.; Laughner, J.; Toon, G.; Wennberg, P.; et al. Using portable low-resolution spectrometers to evaluate Total Carbon Column Observing Network (TCCON) biases in North America. *Atmos. Meas. Tech.* **2023**, *16*, 1239–1261. [CrossRef]